

***PREPARATION AND CHARACTERAZATION
OF COBALT AND COBALT-TITANIUM
SUBSTITUTED BARIUM FERRITES FOR
MAGNETIC RECORDING***

A Thesis submitted

in partial fulfillment of the requirement

for the Degree of

Master of Technology

by

Devendra Kumar Rai

to the

MATERIALS SCIENCE PROGRAMME

INDIAN INSTITUTE OF TECHNOLOGY, KANPUR

July 1999

2 MAR 2000 /MS
CENTRAL LIBRARY
I. I. T., KANPUR

A 130435



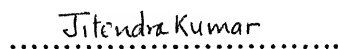
A130435

CERTIFICATE

It is certified that the work contained in this thesis entitled "**Preparation and characterization of cobalt and cobalt-titanium substituted barium ferrites for magnetic recording**", by Devendra Kumar Rai has been carried out under our supervision and that this work has not been submitted elsewhere for a degree.



(K.N.Rai)
Professor
Material Science Programme
& Department of Materials and Metallurgical
Engineering, Indian Institute of Technology,
Kanpur



(Jitendra Kumar)
Professor
Material Science Programme
Indian Institute of Technology,
Kanpur

July 1999

Acknowledgement

I am deeply indebted to my supervisor Prof. Jitendra kumar and Prof.K.N.RAI for their inspiring guidance. I am very fortunate that as I had been under their tutelage. Both constantly encouraged me and the freedom that I got was absolutely remarkable.

It is my pleasure to express my sincere gratitude to Dr.H.C.Verma for his invaluable guidance and continuous encouragement during the course of investigation.

I am very grateful to Shiv Govind, Chandan, Srikanth, Bala, Mini Grover and Vineet Sharma for their valuable suggestions and help towards the completion of this work.

I would like to thank my friends Narsimhan, Amit Srivastava, K.K.Mani Pandey, Rajan Pandey, Pankaj Diwedi, Rama Krishna, Akash Singh, Santosh Sahoo, Manoj Patra and Sanjeev Suman, without which it was difficult for me to regular in my work.

I am giving special thanks to Uma shankerji and Agnihotriji for their constant help through out the experiments.

Thanks are due to my friends who gave a memorable and enjoyable company throughout my stay here.

Devendra Kumar Rai

ABSTRACT

Cobalt and Cobalt-titanium containing barium hexaferrites of compositions $\text{BaFe}_{12-x}\text{Co}_x\text{O}_{19-x/2}$ ($0 < x < 1.6$) and $\text{BaFe}_{12-2x}\text{Co}_x\text{Ti}_x\text{O}_{19}$ ($0 < x < 1.0$) have been prepared by using autoignition method and characterized by X-ray Diffraction (XRD), vibrating sample magnetometer and Mossbauer spectroscopy. It is shown that $\text{BaFe}_{12-x}\text{Co}_x\text{O}_{19-x/2}$ samples though maintain magneto-plumbite hexagonal structure even though another phase of composition $\text{Ba}_2\text{Co}_2\text{Fe}_{12}\text{O}_{22}$ appears when cobalt content (x) becomes 1.2 or more. Their Curie temperatures being 460- 441°C (decreases with cobalt content upto $x=1.2$) and 323°C, respectively. Further, coercivity (H_c) value is found to decrease considerably with rise in cobalt content (x), i.e., from 4223 Oe to 2072 Oe as x varies from zero to 1.6. However, saturation magnetization (M_s) is shown to initially increase marginally but decrease somewhat beyond $x=1.2$, possibly due to emergence of another phase. Moreover, it is determined that Co^{2+} ions replace iron species at 12k and 2b sites preferentially and $4f_{\text{VI}}$, 2a, $4f_{\text{IV}}$ sites randomly. The hyperfine fields of all crystallographic sites except '2b' are found to decrease with increase of cobalt content.

$\text{BaFe}_{12-2x}\text{Co}_x\text{Ti}_x\text{O}_{19}$ compounds also exhibit magneto-plumbite hexaferrite structure. However, particles assume preferred orientation (textured nature) as $\text{Co}^{2+}\text{-Ti}^{4+}$ content increases. In contrast to cobalt alone, $\text{Co}^{2+}\text{-Ti}^{4+}$ substitution is shown to cause enormous decrease in coercivity (H_c) and significant change in Curie temperature (T_c) with no or marginal decrease in saturation magnetization (M_s); their values for $x=0$ and 1 being 4223 and 407 Oe, 460 and 362°C, 58.8 and 56.2 emu/g, respectively. These variations

have been attributed to the preferential filling of 12k, 2b and 4 f_{iv} iron sites by Co²⁺ and non-magnetic Ti⁴⁺ ions. Moreover, hyperfine fields of 12k and 2b sites are shown to remain constant whereas that of 4f_{vi}, 2a and 4f_{iv} sites decrease with increase in Co²⁺-Ti⁴⁺ content. A correlation has also been made between occupancy of iron sites by Co²⁺ and Co²⁺-Ti⁴⁺ ions in modified barium ferrites and resulting magnetic properties. The compounds BaFe_{12-2x}Co_xTi_xO₁₉ with x=0.4- 1.0 are found to conform with the desired characteristics of magnetic recording media, e.g, coercivity and saturation magnetization in the range 1600-407 Oe and 61.1-56.2 emu/g, respectively.

CONTENTS

Certificate.....	ii
Acknowledgement.....	iii
Abstract.....	v
Contents.....	vi
List of figures.....	ix
1. INTRODUCTION.....	1
1.1 Recording medium characteristics.....	2
1.2 Longitudenal and perpendicular recording.....	6
1.3 Preparation techniques.....	8
1.4 Recording media.....	9
1.5 Barium ferrite.....	12
1.6 Objective of the present work.....	17
2. EXPERIMENTAL.....	18
2.1 Preparation of compound.....	18
1.1.1 Cobalt substitution.....	19
1.1.2 Cobalt and titanium substitution.....	20
2.2 Sample characterization.....	20
2.2.1 X-Ray Diffraction.....	20
2.2.2 Magnetic measurements.....	21
2.2.3 Mossbauer spectroscopy.....	22
3. RESULTS AND DISCUSSIONS.....	23
3.1 Cobalt substitution.....	23
3.1.1 X-Ray diffraction analysis.....	23
3.1.2 Magnetic measurements.....	34
3.1.3 Mossbauer spectroscopic analysis.....	44
3.2 Cobalt and titanium substitution.....	50
3.2.1 X-Ray diffraction analysis.....	50
3.2.2 Magnetic measurements.....	58
3.2.3 Mossbauer spectroscopic analysis.....	64
CONCLUSIONS.....	73
REFERENCES.....	74

LIST OF FIGURES

1. Switching field distribution of a magnetic material.....	3
2. Simple model for magnetization transitions in perpendicular and longitude recording.....	7
3. Unit cell of $\text{BaFe}_{12}\text{O}_{19}$ showing the polyhedra co-ordination for Fe in fiv and fvi sites.....	12
4. The $\text{BaFe}_{12}\text{O}_{19}$ structure (a) unit cell with distribution of species (b) closed packed layer sequence with location of iron ions.....	16
5. XRD pattern of cobalt substituted barium ferrite of $\text{BaFe}_{12-x}\text{Co}_x\text{O}_{19}$ ($x =$ 0.2, 0.4, 0.6 and 0.8).....	24
6. XRD pattern of cobalt substituted barium ferrite $\text{BaFe}_{12-x}\text{Co}_x\text{O}_{19}$ ($x = 1.0,$ 1.2, 1.4 and 1.6).....	25
7. Magnetization versus applied field curve for cobalt substituted barium ferrite $\text{BaFe}_{12-x}\text{Co}_x\text{O}_{19}$ ($x = 0.4, 0.8, 1.0, 1.2$ and 1.6).....	35
8. Variation of saturation magnetization with cobalt content in BaFe_{12-x} Co_xO_{19} ($x = 0.4, 0.8, 1.0, 1.2$ and 1.6).....	36
9. Variation of coercivity with cobalt content in $\text{BaFe}_{12-x}\text{Co}_x\text{O}_{19}$ ($x = 0.4,$ 0.8, 1.0, 1.2 and 1.6).....	36
10. Variation of magnetization with temperature for pure and cobalt substituted barium ferrite ($x = 0, 0.2$ and 0.6).....	37
11. Variation of magnetization with temperature for pure and cobalt substituted barium ferrite ($x = 0, 1.0, 1.2$).....	38
12. Variation of magnetization with temperature for pure and cobalt substituted barium ferrite ($x = 0, 1.4$ and 1.6).....	39
13. Variation of dM/dT with temperature for pure and cobalt substituted barium ferrite ($x = 0, 0.2$ and 0.6).....	40

14. Variation of dM/dT with temperature for pure and cobalt substituted barium ferrite ($x = 0, 1.0, 1.2$).....	41
15. Variation of dM/dT with temperature for pure and cobalt substituted barium ferrite ($x = 0, 1.4, 1.6$).....	42
16. Mossbauer spectra of cobalt substituted barium ferrite $BaFe_{12-x}Co_xO_{19}$ ($x = 0, 0.2, 0.4$).....	45
17. Mossbauer spectra of cobalt substituted barium ferrite $BaFe_{12-x}Co_xO_{19}$ ($x = 0.6, 0.8, 1.0$).....	46
18. Mossbauer spectra of cobalt substituted barium ferrite $BaFe_{12-x}Co_xO_{19}$ ($x = 1.2, 1.4, 1.6$).....	47
19. Variation of hyperfine fields of different sites with cobalt contents in $BaFe_{12-x}Co_xO_{19}$ ($x = 0, 0.2, 0.4, 0.6, 0.8, 1.0, 1.2, 1.4, 1.6$).....	49
20. XRD pattern of cobalt and titanium substituted barium ferrite $BaFe_{12-2x}Co_xTi_xO_{19}$ ($x = 0.2, 0.4, 0.6$).....	51
21. XRD pattern of cobalt and titanium substituted barium ferrite $BaFe_{12-2x}Co_xTi_xO_{19}$ ($x = 0.8, 1.0$).....	52
22. Magnetization versus applied field curve for cobalt and titanium substituted barium ferrite $BaFe_{12-2x}Co_xTi_xO_{19}$ ($x = 0.2, 0.4, 0.6, 0.8, 1.0$).....	59
23. Variation of saturation magnetization with cobalt and titanium content in $BaFe_{12-2x}Co_xTi_xO_{19}$ ($x = 0, 0.2, 0.4, 0.6, 0.8, 1.0$).....	60
24. Variation of coercivity with cobalt and titanium content in $BaFe_{12-2x}Co_xTi_xO_{19}$ ($x = 0, 0.2, 0.4, 0.6, 0.8, 1.0$).....	60
25. Variation of Neel temperature with cobalt and titanium content in $BaFe_{12-2x}Co_xTi_xO_{19}$ ($x = 0, 0.2, 0.4, 0.6, 0.8, 1.0$).....	61
26. Variation of magnetization with temperature for cobalt and titanium substituted barium ferrite $BaFe_{12-2x}Co_xTi_xO_{19}$ ($x = 0, 0.4, 0.6, 1.0$).....	62

27. Variation of dM/dT with temperature for cobalt and titanium substituted barium ferrite $BaFe_{12-2x}Co_xTi_xO_{19}$ ($x = 0, 0.4, 0.6, 1.0$).....	63
28. Mossbauer spectra of cobalt and titanium substituted barium ferrite $BaFe_{12-2x}Co_xTi_xO_{19}$ ($x = 0, 0.2, 0.4$).....	65
29. Mossbauer spectra of cobalt and titanium substituted barium ferrite $BaFe_{12-2x}Co_xTi_xO_{19}$ ($x = 0.6, 0.8, 1.0$).....	66
30. Variation of hyperfine fields of different sites with cobalt and titanium content in $BaFe_{12-x}Co_xTi_xO_{19}$ ($x=0, 0.2, 0.4, 0.6, 0.8, 1.0$).....	69

CHAPTER 1

INTRODUCTIONN

Magnetic recording technology in conjunction with semiconductor electronics has contributed significantly to the growth of inexpensive computer power and audio and video storage in the recent past. In magnetic recording there is essentially a device (usually an electromagnetic transducer called 'head') that converts electrical signal into magnetic fields and, in turn, magnetize the medium. The transducer consists of a small coil through which current passes and a gapped magnetic structure to intensify and localize the resulting magnetic field. The medium is a magnetic material coated onto a tape, disk, cylinder, etc. and moves relative to the head in close proximity by maintaining a gap. The head field magnetizes the magnetic species according to current in the coil such that the time varying electrical signal gets converted into a spatially varying magnetic pattern along a track on the medium surface. Reversal of current causes flip over and produces transition between the regions of opposite magnetization. The read back process involves movement of medium (e.g., tape) once again over the head. Now, the field of magnetized region gives rise to a flux in the head coil and a voltage, in turn, gets induced in accordance with the magnetization level of the moving medium. Thus, a spatially varying magnetic pattern is converted back in to a time varying electrical signal [1].

In magnetic recording the encoding of information can be analog or digital type. In analog type, the pattern of magnetization on recording medium should be true representative of the incoming information so that the signal on reading back gives an exact reproduction of the original message. In digital case, information is converted into a sequence of ones and zeroes and recorded to represent regions of opposite magnetization. While the former has been widely used to store audio and video information, the latter is confined to data storage. The picture is changing and digital recording has become popular increasingly in audio and video recording as well, principally, because of the possibility of making dynamic corrections to reconstruct and copy repeatedly. Irrespective of the nature of recording properties requirements of the recording material are similar, though not identical.

1.1 RECORDING MEDIUM CHARACTERISTICS

Any material exhibiting remnant induction after being subjected to magnetic field can be considered a potential recording medium. The retentivity of medium is actually a measure of the magneto motive force available to produce a signal, i.e., material with high retentivity produces high output signals and is therefore preferred. However, the shape of the demagnetization curve is also important, particularly, where short wave length data are to be recorded . The other property relates to field strength needed to cause magnetic reversal, i.e., coercivity (H_c). Its value must not be too large to prevent successful writing and possibly overwriting or erasure by available heads. It must, however, be large enough to resist undesirable changes or degradation of signal using storage possibly by internal or self-

demagnetizing field. This field being proportional to magnetization intensity of media itself, coercivity needs to be high in strongly magnetizable coatings. The internal demagnetization field is important in high density recording when opposite magnetic poles exist in close proximity to each other. Higher coercivity values needed with increasing recording density levels. In addition, the breadth of dM/dH versus H curve is also crucial. This is commonly expressed as switching field distribution (SFD) [2]. A narrow SFD facilitates the writing of sharp and well-defined magnetic transitions enabling information recording at high densities(fig.1). A broad SFD corresponds to not only diffuse transition but also a variety of adverse effects such as erasure, overwriting, etc. The appropriate SFD is important in systems requiring thorough erasure of information using special heads (e.g., analog recording) and in others where some residual overwritten signal can be tolerated but no erase head is used (e.g., digital recording case).

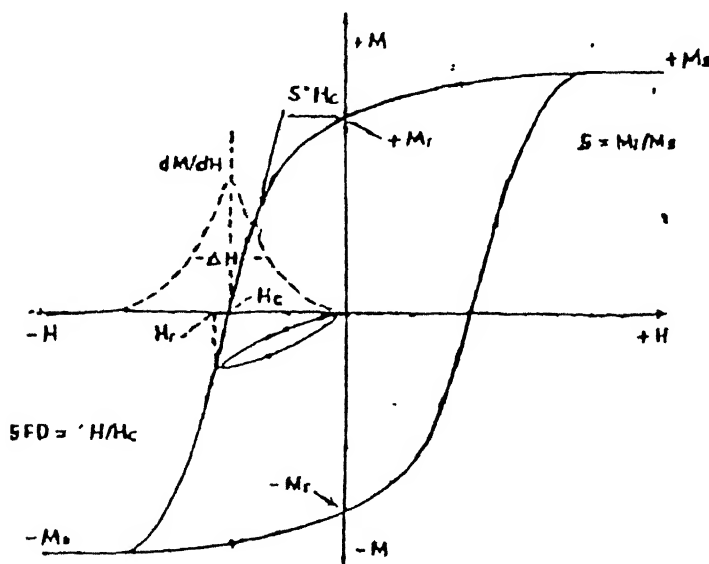


Figure 1. The coercivity H_c is an average property and must be supplemented with switching field distribution, $\Delta H/H_c$ which can be measured by dM/dH versus H curve using the hysteresis loop.

The above magnetic properties of recording medium must be stable under the conditions that prevail during storage. Temperature, relative humidity and atmospheric pollutants provide significant threat in this regard, e.g., strong temperature dependence of coercivity can endanger signal stability and also create difficulties during adjustments of writing and erasing head fields. The overwriting capability can be critically affected in situations where data is originally recorded at a different temperature. Digital equipment such as disk drive can face temperature induce problems because of the heat generated internally by motors and other components. Finally, the temperature at which spontaneous magnetization disappears (i.e., Curie temperature T_c) of recording media must be safely nearly 50°C higher to that likely to prevail during use, transportation or storage of recording medium.

The characteristics discussed so far relate to the bulk or macroscopic magnetic properties. However, the microstructure is equally important. Recording media must contain rigidly held small discrete magnetic units that are partially, if not fully, independent of each other to ensure stable transition between different directions of magnetization in the recorded pattern. Each magnetized segment in the written record must contain enough sub units to make signal to noise ratio adequate. Also, signal to noise ratio is proportional to \sqrt{n} , where n is the density of particle (i.e., number per cm^3). This demands that a good recording media should contain a large number of small size particles. Another reason for making particles as small as possible is to render surface of recording media very smooth. The spacing (d') between the head and the medium is yet another important

parameter in magnetic recording. The loss encountered varies as exponential function of separation to recorded wavelength (d'/λ) ratio. This amounts to 44 (d/λ) dB and 55 (d/λ) dB during writing and reading, respectively [2]. The enormous loss involved in increasing the recording density (i.e., by decreasing the wavelength) without being able to reduce the separation between head and medium are without doubt the critical limiting factor today, e.g., at a density of mere 50,000 bits per inch corresponding to the wavelength of $1\mu\text{m}$, a separation (d') of $0.125\mu\text{m}$ between head and tape during writing and reading is sufficient to cause a loss of 75% of available signal. Moreover, such a close separation is difficult to achieve repeatedly. Although recording performance gets always improved by reducing the head-medium spacing, yet, there is increased likelihood of "head crash" or possibility of mutually destructive contacts between the two. So, a balance must exist between recording performance on one hand and ease of media interchange, durability and longevity on the other. Reduction of head-medium separation requires the right aerodynamic design of the head and appropriate surface finish of the medium as well. The best surface is not necessarily a smooth one as important functional factors of durability, friction and striction are usually found to be optimal when the medium surface is not mirror like. The preparation process involved produce invariably a distribution of particle size with a mean value for recording media. Since signal to noise ratio is improved by reducing the average particle size there is increasing possibility of sizable number to behave like super paramagnetic, not useful at all for recording purposes. We need particles to be small enough so that 10^{14} - 10^{15} can be packed in each cubic centimeter but not so small to become unstable magnetically.

1.2 LONGITUDENAL AND PERPENDICULAR RECORDING

The recording may be done by causing magnetization of the media along any of its three dimensions. It is termed perpendicular, transverse and longitudinal recording when the magnetization is in the direction of its media thickness, across the medium at right angles to its motion, and along the direction of motion, respectively. Longitudinal recording was first exploited in early stages. However, according to Iwasaki and Takemura [3] high-density recording inhibited by nucleation of flux closure inside the media. This flux closure phenomenon is known as Circular magnetization mode and was epoch making. Its observation eventually led to the invention of perpendicular recording. In high density recording, when the current is increased, the magnetization occurs in such a way that magnetic flux tends to close by itself inside the medium and the flux available for reproduction gets reduced. So, in order to attain high density, recording generation of the circular magnetization needs to be suppressed [4]. For this, one way is to have recording with an enhanced longitudinal magnetization component by making the media extremely thin (e.g., use magnetic thin films) so that the longitudinal magnetization is forced to lie in its plane itself. This gives media a strong shape anisotropy. Also, with decrease in film thickness, the magnetization transition becomes sharp. Another way involves recording with an enhanced perpendicular magnetization component. In this case, the magnetization is forced in the direction perpendicular to media plane thereby inhibiting flux closure and leading to sharp magnetization transition.

Fig 2. Show magnetization transitions for perpendicular and longitudinal recordings. Assuming an ideal situation, initial magnetization distributions for isolated transitions are given by step changes M_1 and M_4 for perpendicular and longitudinal recordings, respectively. At this stage, the demagnetized fields H_{d1} for M_1 and H_{d2} for M_4 are induced. Regions where field exceeds the medium coercivity will be subjected to demagnetization, reducing shaded area shown in Fig 2. For perpendicular recording the region around the transition centre remains unchanged, resulting in sharp transition M_2 . For longitudinal recording, the region around the transition center is demagnetized, leading to broad transition M_3 . Thus, the sharp and diffuse magnetization transitions in perpendicular and longitudinal recording respectively are intrinsic properties originating from the difference in the nature of demagnetization alone.

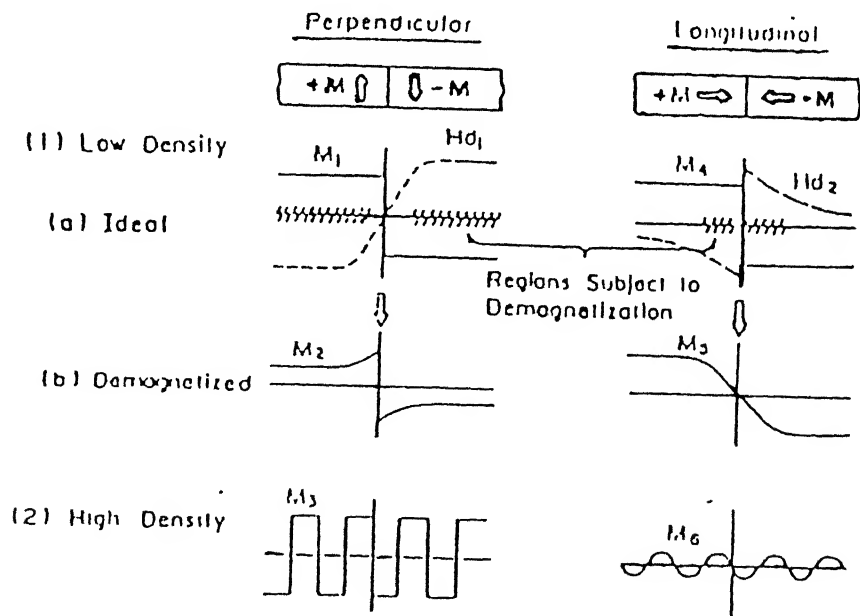


Figure 2 Simple model for magnetization transitions in perpendicular and longitudinal recording

A high magnetostatic energy means that Magnetization State for bit is unstable, i.e., magnetization tends to rotate to cause overall reduction in its value. In order to maintain the magnetization in the desired direction, the magneto static energy must be reduced or anisotropy energy must be increased to counter balance the magnetostatic energy. When a 0.3 - 0.5 μ m thick medium is used for perpendicular recording mode at densities ranging from 50 -100 K FRPI, the corresponding longitudinal recording media having the same magneto static energy should be less than 300 -500 $^{\circ}$ A in thickness, i.e., one order of magnitude thin [5]. The fact that the medium must be thin for high density longitudinal recording causes difficulties: (i) fabrication of uniform corrosion-resistive films, (ii) increase in drop out and, (iii) decrease in reproduced signal amplitude due to reduced magnetic moment per bit [4,6]. Thus, longitudinal recording has a practical upper limit in terms of high density and for ultra high densities (\sim 5 Gb/sq.in.), perpendicular magnetization is only suitable mode of recording.

1.3 PREPARATION TECHNIQUES

There are two major techniques of the preparation of magnetic recording media, termed as "particulate" and "thin film". Each produces a layer of magnetic species on the surface of a non-magnetic support material such as plastic film for tapes, flexible floppy disks, etc. or aluminium plate for rigid disks. The newer method entails deposition of thin films of oxide, pure metal, or alloy on the support by thermal evaporation, sputtering or chemical plating [7]. The above two techniques yield recording media having distinctly different properties. Those produce via thin film

technology exhibit nearly ideal magnetic properties. Such coatings can be very smooth and thin if the support has adequate surface characteristics. They can have very high magnetization intensities because of absence of organic components generally used with discrete particles. Thin films, however, pose practical difficulties in production and have limited use. The particulate media, on the other hand, have large base of infrastructure for manufacturing them at low cost and immense experience for their applications. A few important technique include ceramic, co-precipitation, sol-gel, glass-crystallization and auto ignition and are described in detail elsewhere [8, 9, 10, 11, 12, 13].

1.4 RECORDING MEDIA.

The first commercially available magnetic recording tape was produced in the late 1940 using iron oxide particles. Gamma Ferric oxide ($\gamma\text{-Fe}_2\text{O}_3$), being the most useful among various oxides because of its high chemical and physical stability, has retained an important position today in audio and computer tapes and in flexible and rigid disks industry. Particles size, shape and formation technique of $\gamma\text{-Fe}_2\text{O}_3$ have been greatly improved in last five decades. The particles in use are of acicular shape, contributing significantly to anisotropy. Also, the magnetostatic energy becomes the least when direction of magnetization is collinear with the particle longest dimension [4]. Low coercivity values (usually 300-400 Oe) of $\gamma\text{-Fe}_2\text{O}_3$, however, cause a serious limitation in recording density as the level increases. The requirement of high coercivity was met in mid 1960's with the introduction of chromium dioxide (CrO_2) particles as magnetic

species. Like γ - iron oxides, CrO_2 particles are magnetically uniaxial and derive their anisotropy characteristics from their crystallinity and acicular shapes. Further, the particles exhibit high perfection and uniformity in shapes leading to efficient packing and orientation buildup when coated on polymer tapes. The recent development centres on the control of particle size and coercivity by insertion of iron, antimony, rhodium and iridium in CrO_2 [14,15]. Iridium doped CrO_2 particles available commercially today have coercivity in the range of 500-600 Oe, magnetization intensities of 350-400 emu/cm³ and low Curie temperature of 125°C. But, they are three to four times costlier to $\gamma\text{-Fe}_2\text{O}_3$. Chromium dioxide is used in computer audio-tapes, video cassettes and data recording cartridges. However, its production process requires high pressures. CrO_2 particles are quite abrasive and also somewhat reactive. Their chemical and physical stability is achieved through coatings of appropriate organic components. Nevertheless, low Curie temperature ($\sim 125^\circ\text{C}$) permits fabrication of CrO_2 tapes for use in thermo magnetic and duplication-enabling copying of video information at high speeds.

The current requirements in audio, video and data disks call for materials of high coercivity (1000-2500 Oe). As the wavelength or bit length reduces, demagnetizing field increases, but, the process can be resisted by high coercivity [16]. The magneto crystalline anisotropy constant is known to get tripled by substituting four percent (4%) of iron with cobalt in $\gamma\text{-Fe}_2\text{O}_3$ and, in turn, causes increase in coercivity [17]. But, the particles in the process assume nearly spherical shape lowering acicularity level. Also, the coercivity then becomes very sensitive to

temperature and pressure. Cobalt substituted $\gamma\text{-Fe}_2\text{O}_3$ particles are now widely used as magnetic recording media. The main reason lies in exploiting both the high magneto crystalline anisotropy with stability and high acicularity of $\gamma\text{-Fe}_2\text{O}_3$ particles by confining impregnation of small amount (~2-3 wt %) of cobalt to subsurface regions [12].

The main attraction of using metals and alloys rather than oxides as recording media lies in their extend capacity to the range of choice of magnetization and coercivity [19]. Pure iron has a saturation magnetization of 1700 emu/cm^3 compared with 400 emu/cm^3 for $\gamma\text{-Fe}_2\text{O}_3$. When anisotropy contribution is predominantly due to particle shape, the coercivity becomes directly proportional to magnetization. So, the coercivity of acicular particles of iron should be about 2.5 times higher than that of $\gamma\text{-Fe}_2\text{O}_3$. In fact, high coercivity (1100-1700 Oe) iron particles are now commercially available. However, metal particles are usually susceptible and tend to (i) corrode in atmosphere and (ii) react with the binders. The particles having coercivity value of ~1000 Oe exhibit high signal to noise ratio and are therefore used in audio tape and 8 mm video tapes. Those having coercivity of ~1500 Oe have potential use in high-density flexible disks [20]. Currently, the concentration is primarily on advanced metal particles (MP) and barium ferrite particulate tapes. MP usage is limited to densities of 100 kfc/i due to their large size and associated low coercivity values. New MP^{++} tapes utilizing much smaller particles with significantly higher magnetization and coercivity offer much better performance. Though metallic particles are popular, barium ferrite is replacing them at ultra high densities (5Gb/sq.in.) following the

development of giant magneto resistance heads. It provides excellent media for perpendicular recording by utilizing its hexagonal shape platelet type particles and magnetization easy axis along the thickness. Besides, they can be mass produced with the prevailing infrastructure and used with the available head-medium interface technologies. Another advantage is its oxidation or corrosion resistance characteristics.

1.5 BARIUM FERRITE

The barium ferrite $\text{BaFe}_{12}\text{O}_{19}$ has a magneto plumbite structure with hexagonal unit cell having parameter $a=5.892 \text{ \AA}$, $c=23.183 \text{ \AA}$, $Z=2$ and space group $p6_3/mmc$ [21]. The unit cell consists of S and R blocks in sequence of RSR^*S^* where asterisks indicate a 180 degree rotation with respect to c-axis Fig 3. The R block in this case is formed by the group $(\text{BaFe}_6\text{O}_{11})^{2-}$ whereas S block comprises of $(\text{FeO}_8)^{2+}$ and has no barium cations. The oxygen has a cubic close packing configuration (i.e., ABCABC..) in the S block and hexagonal layer sequence (i.e., ABAB..) in the R block. The $[111]$ cubic axis coincides with the $[0001]$ hexagonal axis. Fe^{3+} ions occupy five types of crystal sites. There are 12 octahedral k-sites, four tetrahedral f_{iv} (or f_2) sites and two 'b' sites having a five-fold symmetry [fig 3]. The R and S units share the 12 iron ions in k sites. The four f_{vi} are in R block close to Ba^{2+} ions and forming a Fe_2O_9 group of two octahedra with a common face. The two 'a' sites are present in S block. The two 'b' sites with five-fold symmetry are formed by two tetrahedral sharing a common face. A detailed XRD study showed that Fe ions lie in a double well potential of the bipyramid centre.

Figure 4 shows the unit cell together with layer sequence and distribution of various species. Twenty four Fe^{3+} ions occupy the positions as given in Table 1.

Table 1: Positions of Fe^{3+} ions in hexagonal unit cell of barium ferrite.

Site	No. of position	co-ordinates
2a	2	0,0,0; 0,0,1/2
2b	2	0,0,1/4; 0,0,3/4
4f	8	$\pm(1/3, 2/3, z; 2/3, 1/3, 1/2 + z)$ $z = 0.028, 0.89$
12k	12	$\pm(x, 2x, z; 2x, x, z; x, x, z; x, 2x, 1/2 - z;$ $2x, x, 1/2 + z; x, x, 1/2 + z)$

The Fe^{3+} ions configuration, number per formula unit, block location and spin direction are listed in Table 2. There are five distinct crystallographic sites or sublattices $4f_{vi}$, 2b, 12k, $4f_{iv}$ and 2a, for metallic cations. Their crystallographic and magnetic characteristics are given in Table 2. The magnetic species in barium ferrite are twenty-four Fe^{3+} ions, each with moment of $5 \mu_B$ (Bohr magneton). Their moment lie perpendicular to close packed oxygen layers, i.e., parallel or antiparallel to c-axis or [0001] of hexagonal cell. By assuming the known spin directions of Fe^{3+} ions in spinal configuration (or S block) and applying the principles governing the super exchange force, one can proceed from ion to ion through out the cell and predict the direction of its net spin moment, i.e., parallel or antiparallel to [0001]. This suggests spins of 16 ions in one

direction and of 8 in the other. The net magnetic moment per cell should therefore be $(16-8) \times 5 \mu_B = 40 \mu_B$ per cell or $20 \mu_B$ per molecule of $\text{BaFe}_{12}\text{O}_{19}$. This matches well with the experimental value of 100 emu/g [22].

Table 2: Iron ions configuration; number per formula unit, block location and spin direction in barium ferrite $\text{BaFe}_{12}\text{O}_{19}$

Site	Configuration	Number	Block	Spin
4fvi	Octahedral	2	R	down
2b	Bipyramidal	1	R	up
12k	Octahedral	6	R-S	up
4fiv	Tetrahedral	2	S	down
2a	Octahedral	1	S	up

The coercivity (H_c) is due to linear addition of two terms involving local effects of crystal anisotropy through magneto crystalline factor k , and contribution of magnetostatic fields, caused by particle morphology and inter particle interaction through shape anisotropy or demagnetizing factor α [23]. Thus,

$$H_c = \beta(k/M_s) + \alpha M_s$$

Where M_s is saturation magnetization and $\beta(=2)$ is a constant. The second term on the right hand side stands for the contribution of shape anisotropy. For thin platelets $\alpha = -1$ [24, 17]

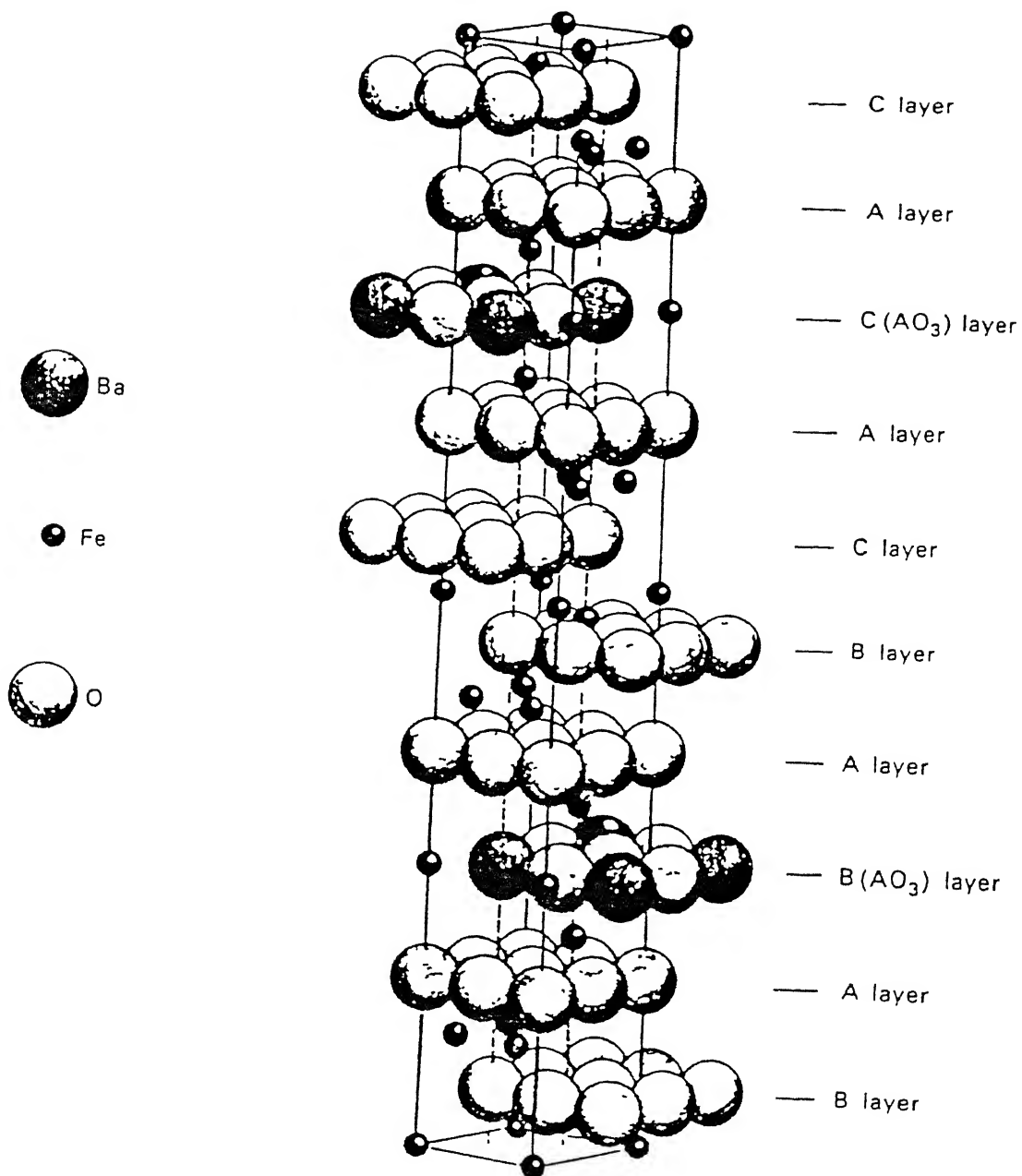


Figure 4 : The closed packed layer sequence with location of iron ions in the $\text{BaFe}_{12}\text{O}_{19}$.

In the case of Barium ferrite crystalline term is predominant and dictates the preferred axis (perpendicular to plate) but, shape anisotropy has opposite effect and if sufficiently strong would make this axis an "unfavoured one for magnetization. This conflict of anisotropy, each with its own temperature coefficient, gives the coercivity of barium ferrite more complicated temperature dependence than the simple monotonic decline seen in acicular particles [23,25].

The final properties of barium ferrite are weakly dependent on the preparation routes as only morphology can be influenced (crystal structure being highly stable). Consequently, recent research has been focussed on the development of a variety of ferrites by partial replacement of iron with metal species [26]. An attempt has been made in the direction in the present study as well.

1.5 OBJECTIVE OF THE PRESENT WORK.

The objective has been to substitute iron partially with cobalt and cobalt-titanium in barium ferrite and prepare compounds of compositions $\text{BaFe}_{12-x}\text{Co}_x\text{O}_{19-x/2}$ and $\text{BaFe}_{12-2x}\text{Co}_x\text{Ti}_x\text{O}_{19}$ taking in steps of 0.2 up to 1.6 and 1.0, by autoignition method and study the resulting effect on structure, phase(s), magnetic characteristics(e.g, specific magnetization, coercivity and curie temperature). The idea has been to obtain information about site occupancy of cobalt in modified barium ferrites and to find out its possible correlation with the associated changes in the magnetic properties for tailer making of corresponds of desirable characteristic

CHAPTER 2

EXPERIMENTAL

In this Chapter, preparation of cobalt and cobalt-titanium containing barium ferrite and their characterization by X-ray diffraction (XRD), magnetic measurement and Mossbauer spectroscopy are described.

2.1 PREPARATION OF COMPOUNDS

Pure barium ferrite $\text{BaFe}_{12}\text{O}_{19}$ has been prepared by mixing appropriate amounts of barium and ferrite nitrates with an aqueous solution of citric acid (maintaining the pH with ethylene diamine at 4.0) and heating to form a gel. Auto ignition combustion, used for preparing Bi-Pb-Sr-Ca-Cu-O superconductor [13] and extended for barium ferrite recently [26], has been employed to obtain ash from the gel. The uniqueness of the process lies in the initiation of combustion at a low temperature and use of the heat liberated by the exothermic anionic oxidation reduction reaction between the citrate and nitrate ions. The calcination of the ash at 900°C - 1000°C for few hours produces the final product. The raw materials, their make and grade used are listed in Table 3.

Cobalt and cobalt-titanium have been partially substituted for iron in barium ferrite to obtain the compound $\text{BaFe}_{12-x}\text{Co}_x\text{O}_{19-x/2}$ and $\text{BaFe}_{12-2x}\text{Co}_x\text{Ti}_x\text{O}_{19}$ and study their effects on magnetic and structural properties.

Table 3: List of raw materials used with make and grade.

Material	Make	Grade
Barium nitrate $[\text{Ba}(\text{NO}_3)_2]$	THOMAS BAKER	L.R
Ferric nitrate $[\text{Fe}(\text{NO}_3)_3 \cdot 9\text{H}_2\text{O}]$	NICE	L.R
Citric acid $\begin{array}{c} [\text{CH}_2\text{-COOH} \\ \\ \text{HO-C-COOH} \\ \\ \text{CH}_2\text{-COOH}] \end{array}$	INTERNATIONAL CHEMICAL INDUSTRIES	A.R
Cobalt nitrate $[\text{Co}(\text{NO}_3)_2 \cdot 6\text{H}_2\text{O}]$	NICE	L.R
Ethylene diamine $[\text{NH}_2\text{-CH}_2\text{-CH}_2\text{NH}_2]$	S.D.FINE CHEMICAL LTD	L.R

2.1.1 COBALT SUBSTITUTION

We have prepared eight types of samples having composition $\text{BaFe}_{12-x}\text{Co}_x\text{O}_{19-x/2}$ by taking values of x as 0.2, 0.4, 0.6, 0.8, 1.0, 1.2, 1.4 and 1.6. For this, we have added appropriate amount of $\text{Ba}(\text{NO}_3)_2$, $\text{Fe}(\text{NO}_3)_3 \cdot 9\text{H}_2\text{O}$ and $\text{Co}(\text{NO}_3)_2 \cdot 6\text{H}_2\text{O}$ to citric acid solution. Ethylene diamine was added drop wise till pH of solution reached a value of 4.0. Solution was then stirred properly and heated to yield ash. The ash was calcined at 1000°C for 8 hours in each case to give the final product.

2.1.2 COBALT-TITANIUM SUBSTITUTION

The five samples prepared correspond to composition $\text{BaFe}_{12-2x}\text{Co}_x\text{Ti}_x\text{O}_{19}$ with $x = 0.2, 0.4, 0.6, 0.8$ and 1.0 . To compensate for charge imbalance resulting due to Co^{2+} , equal number Ti^{4+} ions are added. As no aqueous solution of Ti^{4+} exists, the appropriate amount of TiO_2 powder as added in the mixture of barium-, cobalt- and iron-nitrates and citric acid solution. Also, since TiO_2 is not soluble in water, the proper mixing was ensured by high level of powder dispersion in the solution. To achieve this, the pH of the solution was maintained at 4.0 (this being isoelectric point of TiO_2) by ethylene diammine [27]. Solution was heated to yield ash as before which, in turn, was calcined at 1100°C for 8 hours to get the final product.

2.2 SAMPLE CHARACTERIZATION:

2.2.1 X-RAY DIFFRACTION (XRD)

The XRD patterns of various samples have been recorded in a Rich - Seifert X-ray diffractometer (model ISO Debye flux 2002) using $\text{CuK}\alpha$ radiation to ascertain the nature of barium ferrites and to find out phase(s) present. For this, powder was packed in a 10mm diameter circular cavity of Perspex sample holder, which was then mounted in its position on the diffractometer. The diffracted beam was received by a scintillation counter detector, held at angle of 2θ with the transmitted beam. The X-ray tube was

operated at 30kV and 20mA and XRD pattern recorded at scanning rate of 3°/min and chart speed of 30mm/min. The time constant was 10 seconds and sensitivity was either 5000 or 2000 counts per minute.

2.2.2 MAGNETIC MEASUREMENTS

Initially, 1ml of 1-% polyvinyl alcohol (binder) was added to one gram of ferrite sample and slurry formed was mixed properly in a mortar for fifteen minutes. Subsequently, the slurry was kept in an oven at 90°C for two hours and allowed to cool. A pellet of size 3mm x 3mm x 4mm was then made by using a special die, fabricated for the purpose. All pellets were kept at 400°C for two hours so as to expel the polyvinyl alcohol present. The magnetic moment measurements were carried out with a parallel field vibrating sample magnetometer VSM (Princeton Applied Research Model - 150 A) in conjunction with an electromagnet (varian model V-2700), providing a magnetic field of upto 11.5 K Oe. Also, the magnetic moment versus temperature data was obtained at a fixed magnetic field of 10^4 Oe to determine the Curie temperature of the products. The temperature was set with a controller (Indotherm model 401) and a regulated power supply (Networks model NPS 30/5D). A chromel-alumel thermocouple was held close to the sample to indicate the temperature. The sample chamber was evacuated using a pumping module during the heating process.

The information derived from the measurements at room temperature comprises of specific magnetization M_s , remanance magnetization M_r , and coercive field H_c . The Curie temperature T_c was however determined for pure and some cobalt and cobalt-titanium modified barium ferrite only.

2.2.3 MOSSBAUER SPECTROSCOPY

About 50 mg of each sample was spread uniformly in a circular area of 12-mm diameter and sandwiched between cello tape pieces. A vibrating radioactive source ^{57}Co of strength 5mC embedded in rhodium matrix provided γ -rays to fall on the sample. The transmitted radiation was detected by a gas filled proportional counter. The signal generated was digitized and counts stored in a multichannel analyser. The Mossbauer spectra were in a constant acceleration mode with V_{max} as ± 15 mm/s and calibrating the setup with ^{57}Fe source. Their analysis carried out using a computer programme in FORTRAN language assuming the spectral lines to be of Lorentzian shapes and considering singlets, doublets and sextets contributions separately. The information about the parameters like isomer shifts, quadrupole splitting, line width and internal hyperfine fields were obtained from the Mossbauer spectra.

CHAPTER 3

RESULTS AND DISCUSSION

3.1 COBALT SUBSTITUTION

The size difference between iron and cobalt ions is less than 15%. Moreover, the hexagonal ferrite phase is known to persist with little deviation in stoichiometry even [21]. Therefore, it is expected that while the crystal structure of the compound may not change when a few Co^{2+} ions replace Fe^{3+} ions, magnetic characteristics may get influenced considerably. Also, cobalt being divalent, non-stoichiometry should result for ensuring charge neutrality as a whole. To examine the associated effects, we have partially substituted iron with cobalt by adding different amounts of $\text{Co}(\text{NO}_3)_2 \cdot 6\text{H}_2\text{O}$ to the barium and iron nitrate citrate solution and prepared compound with composition $\text{BaFe}_{12-x}\text{Co}_x\text{O}_{19-x/2}$ (x being ≤ 1.6).

3.1.1 X-RAY ANALYSIS

The XRD pattern of all the samples are shown in Figures 5-6. The d-values and relative intensities of various diffracted peaks along with their indices are given in Table 4-11. For sake of comparison, standard data of $\text{BaFe}_{12}\text{O}_{19}$ are also included in each case. With increased cobalt content the intensity of 20.0, 11.0 and 22.0 diffraction peaks of barium ferrite become increasingly stronger and for sample with $x=1.6$, they are most prominent. The results depict the presence of hexagonal magnetoplumbite structure all through with particles assuming preferred orientation and /or emergence of

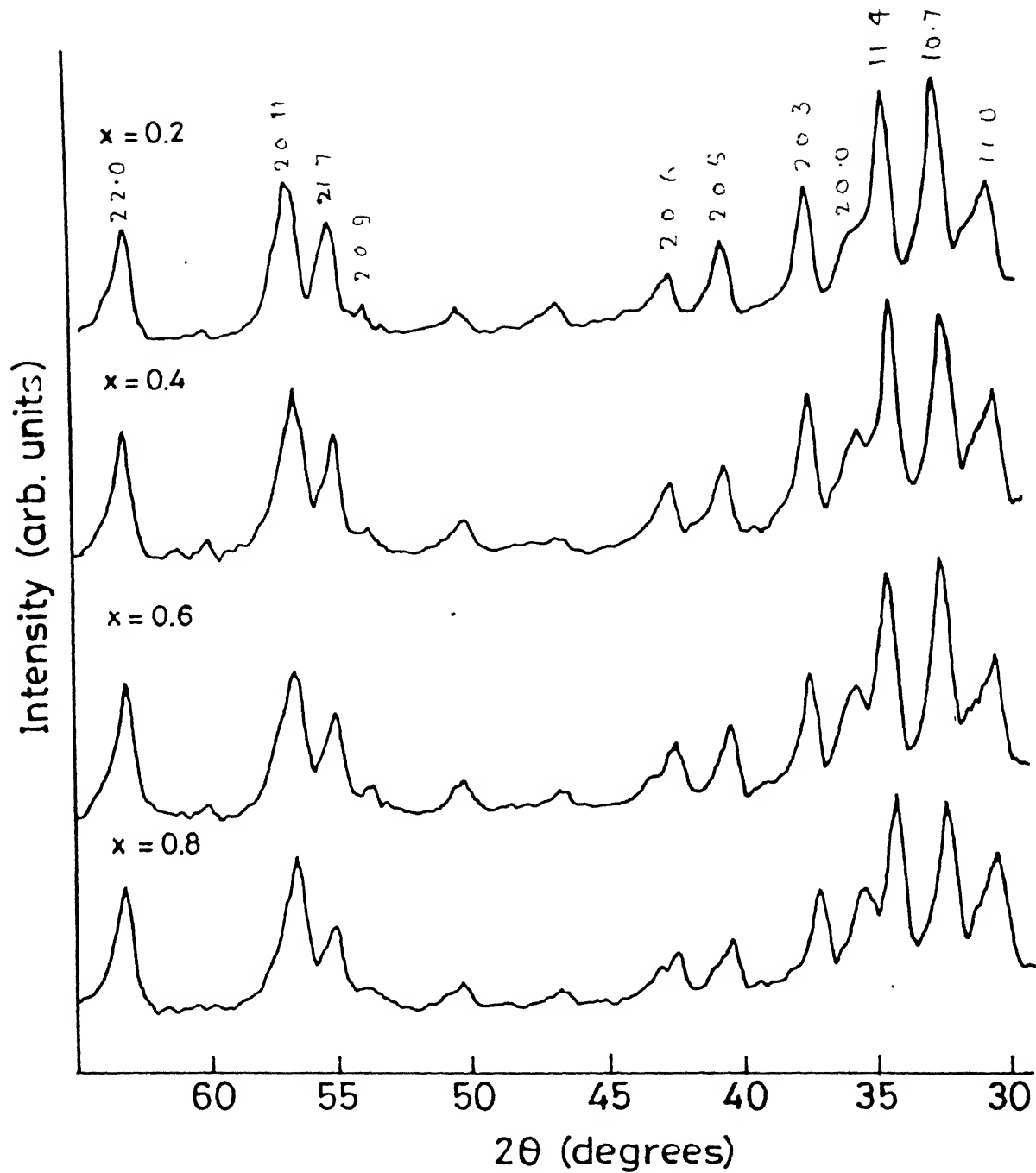
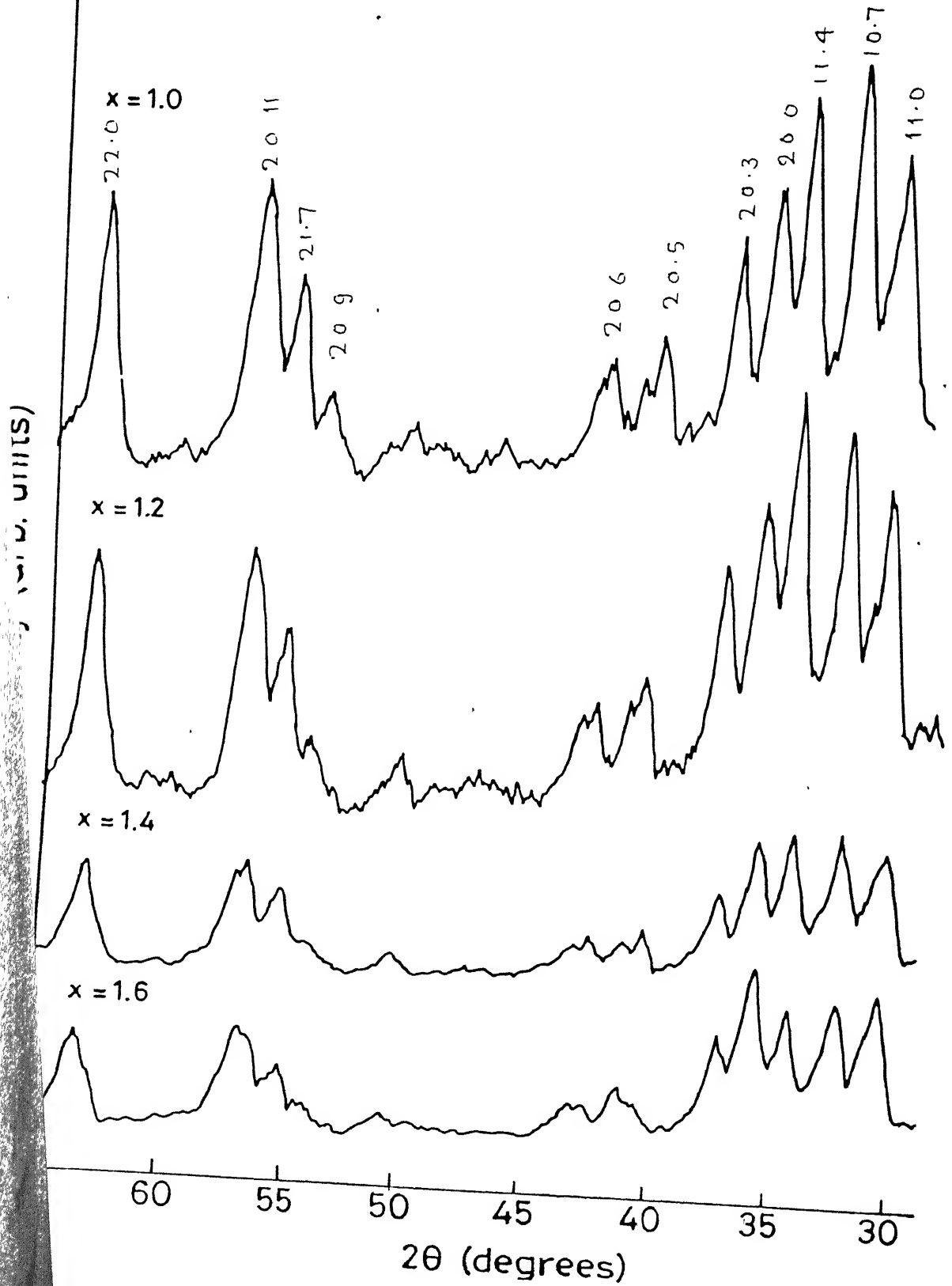


Figure 5: XRD pattern of cobalt substituted barium ferrite $\text{BaFe}_{12-x}\text{Co}_x\text{O}_{19-x/2}$ ($x=0.2, 0.4, 0.6$ and 0.8)



6: XRD pattern of cobalt substituted barium ferrite $\text{BaFe}_{12-x/2}$ ($x=1.0, 1.2, 1.4$ and 1.6)

Table 4 : Interplanar spacings and intensities of various peaks observed in XRD of cobalt substituted barium ferrite $\text{BaFe}_{12-x}\text{Co}_x\text{O}_{19-x/2}$ ($x=0.2$)

d-values for $\text{BaFe}_{12}\text{O}_{19}$ (\AA^0)	Interplanar spacing Observed for $\text{BaFe}_{12-x}\text{Co}_x\text{O}_{19-x/2}$ ($x=0.2$) $d(\text{\AA}^0)$	Intensities For $\text{BaFe}_{12}\text{O}_{19}$	Intensities observed for $\text{BaFe}_{12-x}\text{Co}_x\text{O}_{19-x/2}$ ($x=0.2$)	hk.l indices
2.94	2.92	55	55.95	1 1 . 0
2.78	2.76	100	94.05	1 0 . 7
2.62	2.61	98	100	1 1 . 4
2.42	2.41	60	54.65	2 0 . 3
2.23	2.22	29	31.39	2 0 . 5
2.13	2.12	18	17.44	2 0 . 6
1.81	1.81	10	4.65	2 0 . 9
1.66	1.66	53	44.18	2 1 . 7
1.63, 1.62 1.61	1.62	30,58,10	61.62	2 0 . 11
1.47	1.47	63	45.34	2 2 . 0

The standard data for pure $\text{BaFe}_{12}\text{O}_{19}$ phase is given for sake of comparison.

Table 5: Interplanar spacings and intensities of various peaks observed in XRD of cobalt substituted barium ferrite $\text{BaFe}_{12-x}\text{Co}_x\text{O}_{19-x/2}$ ($x=0.4$)

d-values for $\text{BaFe}_{12}\text{O}_{19}$ ($^{\circ}\text{\AA}$)	Interplanar spacings observed for $\text{BaFe}_{12-x}\text{Co}_x\text{O}_{19-x/2}$ ($x=0.4$) $d(^{\circ}\text{\AA})$	Intensities for $\text{BaFe}_{12}\text{O}_{19}$	Intensities observed for $\text{BaFe}_{12-x}\text{Co}_x\text{O}_{19-x/2}$ ($x=0.4$)	hk.l indices
2.94	2.94	55	60.57	1 1 0
2.78	2.77	100	93.71	1 0 7
2.62	2.62	98	100	1 1 4
2.55	2.53	11	45.15	2 0 0
2.42	2.41	60	61.4	2 0 3
2.23	2.22	29	30.28	2 0 5
2.13	2.13	18	23.42	2 0 6
1.66	1.66	53	47.42	2 1 7
1.63, 1.62, 1.61	1.62	30,58,10	69.71	2 0 11
1.47	1.47	63	50.28	2 2 0

The standard values for pure $\text{BaFe}_{12}\text{O}_{19}$ phase is given for sake of comparison.

Table 6: Interplanar spacings and intensities of various peaks observed in XRD of cobalt substituted barium ferrite, $\text{BaFe}_{12-x}\text{Co}_x\text{O}_{19-x/2}$ ($x=0.6$)

d-values for $\text{BaFe}_{12}\text{O}_{19}$ ($^{\circ}\text{\AA}$)	Interplanar spacings Observed for $\text{BaFe}_{12-x}\text{Co}_x\text{O}_{19-x/2}$ ($x=0.6$)	Intensities for $\text{BaFe}_{12}\text{O}_{19}$	Intensities observed for $\text{BaFe}_{12-x}\text{Co}_x\text{O}_{19-x/2}$ ($x=0.6$)	hkl indices
2.94	2.94	55	55.81	1 1 . 0
2.78	2.77	100	100	1 0 . 7
2.62	2.62	98	93.31	1 1 . 4
2.55	2.53	11	43.60	2 0 . 0
2.42	2.41	60	49.13	2 0 . 3
2.23	2.23	29	26.74	2 0 . 5
2.13	2.13	18	20.93	2 0 . 6
1.66	1.66	53	36.04	2 1 . 7
1.63,1.62, 1.61	1.62	30,58,10	55.81	2 0 . 11
1.47	1.47	63	51.74	2 2 . 0

The standard data for pure $\text{BaFe}_{12}\text{O}_{19}$ phase is given for the sake of comparison.

Table 7 : Interplanar spacings and intensities of various peaks observed in XRD of cobalt substituted barium ferrite $\text{BaFe}_{12-x}\text{Co}_x\text{O}_{19-x/2}$ ($x=0.8$)

d-values for $\text{BaFe}_{12}\text{O}_{19}$ ($^{\circ}\text{\AA}$)	Interplanar spacing observed for $\text{BaFe}_{12-x}\text{Co}_x\text{O}_{19-x/2}$ ($x=0.8$)	Intensities for $\text{BaFe}_{12}\text{O}_{19}$	Intensities observed for $\text{BaFe}_{12-x}\text{Co}_x\text{O}_{19-x/2}$ ($x=0.8$)	hk.l indices
2.94	2.93	55	68.30	1 1 . 0
2.78	2.77	100	96.83	1 0 . 7
2.62	2.62	98	100	1 1 . 4
2.55	2.53	11	51.05	2 0 . 0
2.42	2.42	60	43.66	2 0 . 3
2.23	2.22	29	25.35	2 0 . 5
2.13	2.12	18	19.36	2 0 . 6
1.66	1.66	53	35.91	2 1 . 7
1.63,1.62, 1.61	1.62	30,58,10	73.24	2 0 . 11
1.47	1.47	63	59.50	2 2 . 0

The standard data for pure $\text{BaFe}_{12}\text{O}_{19}$ phase is given for the sake of comparison.

Table 8: Interplanar spacings and intensities of various peaks observed in XRD of cobalt substituted barium ferrite $\text{BaFe}_{12-x}\text{Co}_x\text{O}_{19-x/2}$ ($x=1.0$)

d-values for $\text{BaFe}_{12}\text{O}_{19}$ ($^{\circ}\text{A}$)	Interplanar spacings observed for $\text{BaFe}_{12-x}\text{Co}_x\text{O}_{19-x/2}$ ($x = 1.0$)	Intensities for $\text{BaFe}_{12}\text{O}_{19}$	Intensities observed for $\text{BaFe}_{12-x}\text{Co}_x\text{O}_{19-x/2}$ ($x=1.0$)	hk.l indices
2.94	2.93	55	77.62	1 1 . 0
2.78	2.76	100	100	1 0 . 7
2.62	2.61	98	91.07	1 1 . 4
2.55	2.52	11	68.23	2 0 . 0
2.42	2.41	60	56.96	2 0 . 3
2.23	2.23	29	28.79	2 0 . 5
2.13	2.13	18	22.53	2 0 . 6
1.66	1.66	53	42.88	2 1 . 7
1.63,1.62, 1.61	1.62	30,58,10	67.76	2 0 . 11
1.47	1.47	63	63.22	2 2 . 0

The standard data for pure $\text{BaFe}_{12}\text{O}_{19}$ phase is given for the sake of comparison.

Table 9 : Interplanar spacings and intensities of various peaks observed in XRD of cobalt substituted barium ferrite $\text{BaFe}_{12-x}\text{Co}_x\text{O}_{19-x/2}$ ($x=1.2$)

d-values for $\text{BaFe}_{12}\text{O}_{19}$ ($^{\circ}\text{\AA}$)	Interplanar spacings observed for $\text{BaFe}_{12-x}\text{Co}_x\text{O}_{19-x/2}$ ($x=1.2$)	Intensities for $\text{BaFe}_{12}\text{O}_{19}$	Intensities observed for $\text{BaFe}_{12-x}\text{Co}_x\text{O}_{19-x/2}$ ($x=1.2$)	hkl indices
2.94	2.92	55	75.37	1 1 . 0
2.78	2.77	100	89.63	1 0 . 7
2.62	2.60	98	100	1 1 . 4
2.55	2.52	11	70.87	2 0 . 0
2.42	2.41	60	55.25	2 0 . 3
2.23	2.23	29	26.72	2 0 . 5
2.13	2.12	18	20.57	2 0 . 6
1.66	1.66	53	36.93	2 1 . 7
1.63,1.62, 1.61	1.62	30,58,10	56.75	2 0 . 11
1.47	1.47	63	54.35	2 2 . 0

The standard data for pure $\text{BaFe}_{12}\text{O}_{19}$ phase is given for the sake of comparison.

Table 10: Interplanar spacings and intensities of various peaks observed in XRD of cobalt substituted barium ferrite $\text{BaFe}_{12-x}\text{Co}_x\text{O}_{19-x/2}$ ($x=1.4$)

d-values for $\text{BaFe}_{12}\text{O}_{19}$ ($^{\circ}\text{\AA}$)	Interplanar spacings observed for $\text{BaFe}_{12-x}\text{Co}_x\text{O}_{19-x/2}$ ($x=1.4$)	Intensities for $\text{BaFe}_{12}\text{O}_{19}$	Intensities observed for $\text{BaFe}_{12-x}\text{Co}_x\text{O}_{19-x/2}$ ($x=1.4$)	hk.l indices
2.94	2.93	55	76.91	1 1 . 0
2.78	2.76	100	100	1 0 . 7
2.62	2.61	98	99.21	1 1 . 4
2.55	2.51	11	87.98	2 0 . 0
2.42	2.41	60	56.94	2 0 . 3
2.23	2.22	29	19.81	2 0 . 5
2.13	2.12	18	20.59	2 0 . 6
1.66	1.66	53	43.83	2 1 . 7
1.63,1.62, 1.61	1.62	30,58,10	63.65	2 0 . 11
1.47	1.47	63	59.12	2 2 . 0

The standard data for pure $\text{BaFe}_{12}\text{O}_{19}$ is given for the sake of comparison.

Table 11: Interplanar spacings and intensities of various peaks observed in XRD of cobalt substituted barium ferrite $\text{BaFe}_{12-x}\text{Co}_x\text{O}_{19-x/2}$ ($x=1.6$)

d-values for $\text{BaFe}_{12}\text{O}_{19}$ ($^{\circ}\text{\AA}$)	Interplanar spacings observed for $\text{BaFe}_{12-x}\text{Co}_x\text{O}_{19-x/2}$ ($x=1.6$) ($^{\circ}\text{\AA}$)	Intensities for $\text{BaFe}_{12}\text{O}_{19}$	Intensities observed for $\text{BaFe}_{12-x}\text{Co}_x\text{O}_{19-x/2}$ ($x=1.6$)	hk.l indices
2.94	2.94	55	84.69	1 1 . 0
2.78	2.77	100	95.02	1 0 . 7
2.62	2.62	98	80.22	1 1 . 4
2.55	2.52	11	100	2 0 . 0
2.42	2.42	60	50	2 0 . 3
2.23	2.23	29	22.96	2 0 . 5
2.13	2.13	18	19.38	2 0 . 6
1.81	1.81	10	11.73	2 0 . 9
1.66	1.66	53	48.97	2 1 . 7
1.63,1.62, 1.61	1.62	30,58,10	52.55	2 0 . 11
1.47	1.47	63	51.65	2 2 . 0

The standard data for pure $\text{BaFe}_{12}\text{O}_{19}$ phase is given for the sake of comparison.

another phase possibly $\text{Ba}_2\text{Co}_2\text{Fe}_{12}\text{O}_{22}$, which has a rhombohedral structure. The unit cell parameters on hexagonal axes are $a=5.8596 \text{ \AA}$, $c=43.502 \text{ \AA}$, $Z=3$ and space group $R3m$ [28].

3.1.2 MAGNETIC MEASUREMENT

The Magnetization versus magnetic field curves of cobalt substituted barium ferrites for $x=0.4, 0.8, 1.0, 1.2, 1.6$ at room temperature are shown in figure 7. The values of their saturation magnetization and coercivity are given in Table12.

Table 12: Saturation Magnetization and Coercivity of different cobalt containing barium ferrite $\text{BaFe}_{12-x}\text{Co}_x\text{O}_{19-x/2}$.

Amount of cobalt substitution x	Saturation Magnetization (M_s) (emu/gm)	Coercivity(H_c) (Oe)	Curie Temperature $T(^{\circ}\text{C})$ (a)	Curie Temperature $T(^{\circ}\text{C})$ (b)
0.0	58.7656	4223	481.3	460.8
0.2	-----	-----	483.2	462.4
0.4	59.874	3607	-----	-----
0.6	-----	-----	487.5	458
0.8	60.7689	3119	-----	-----
1.0	61.1983	2816	492.4	452.7
1.2	59.1972	2639	495.7	441.7
1.4	-----	-----	499.3	452.2
1.6	54.2207	2082	506.1	453.9

a) Intersection of tangent at largest slope with X-axis

b) Minima of dM/dT vs Temperature plots

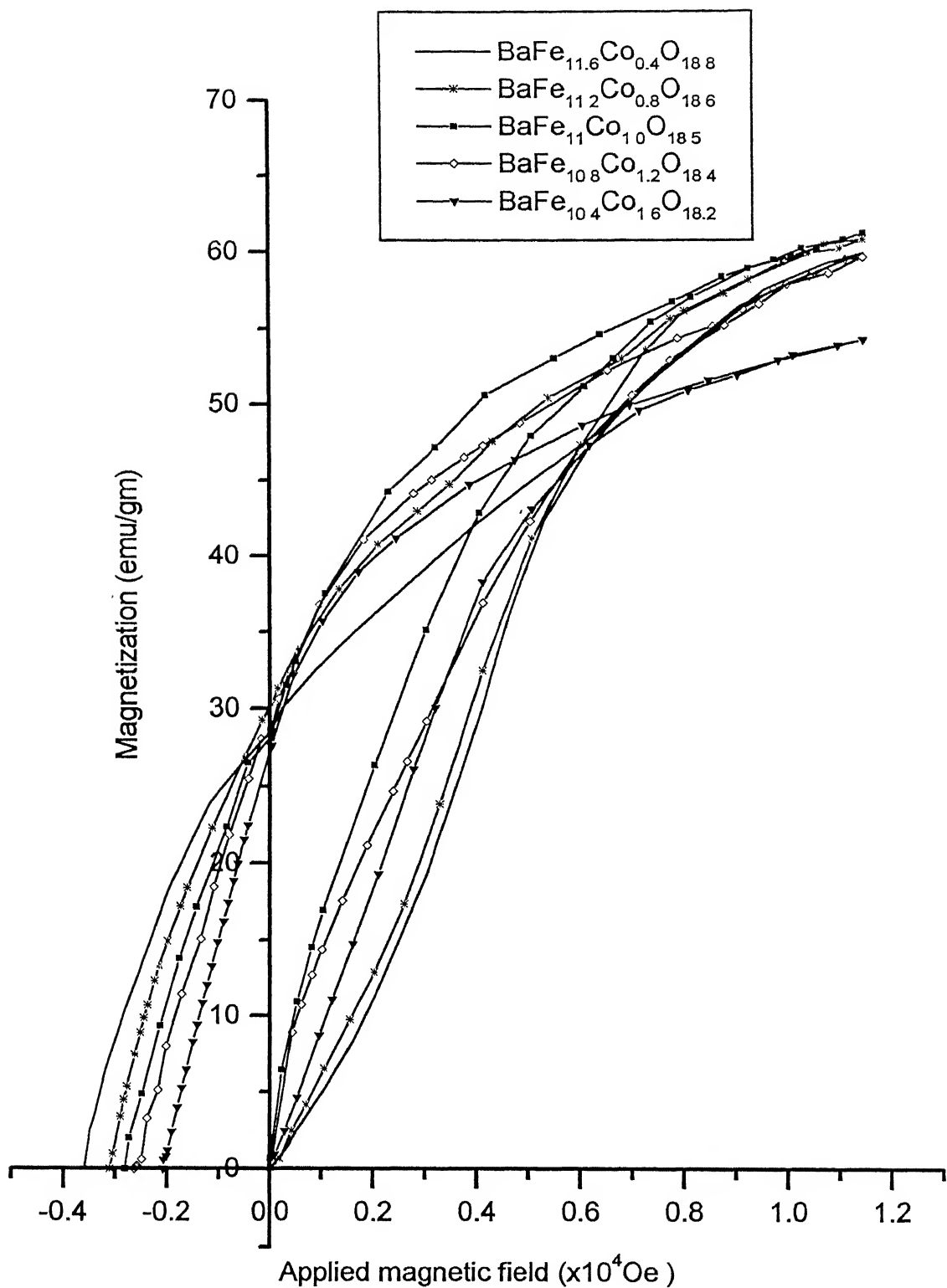


Figure 7: Magnetization versus applied field curve for cobalt containing barium ferrite $\text{BaFe}_{12-x}\text{Co}_x\text{O}_{19-x/2}$ ($x=0.4, 0.8, 1.0, 1.2$, and 1.6)

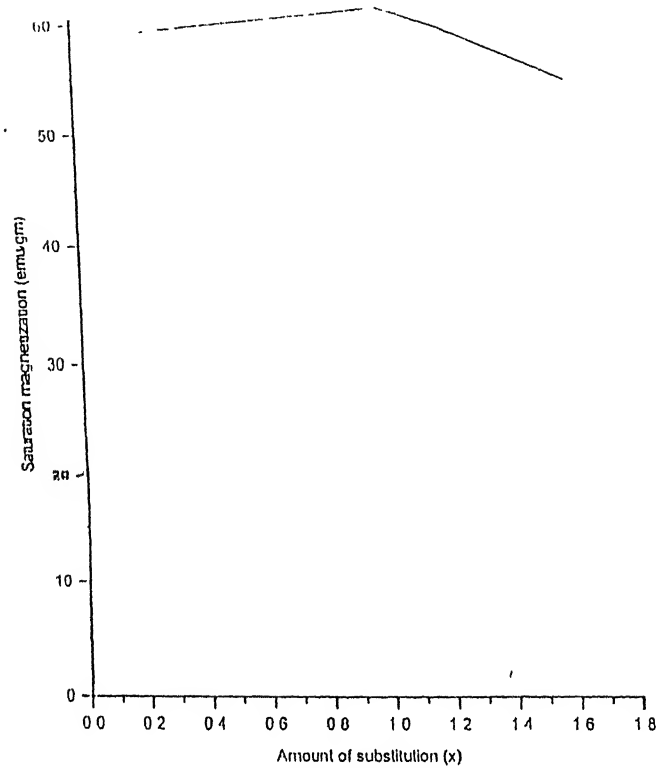


Figure 8 Saturation magnetization for $\text{BaFe}_{12-x}\text{Co}_x\text{O}_{19-2x}$ as a function of substitution x

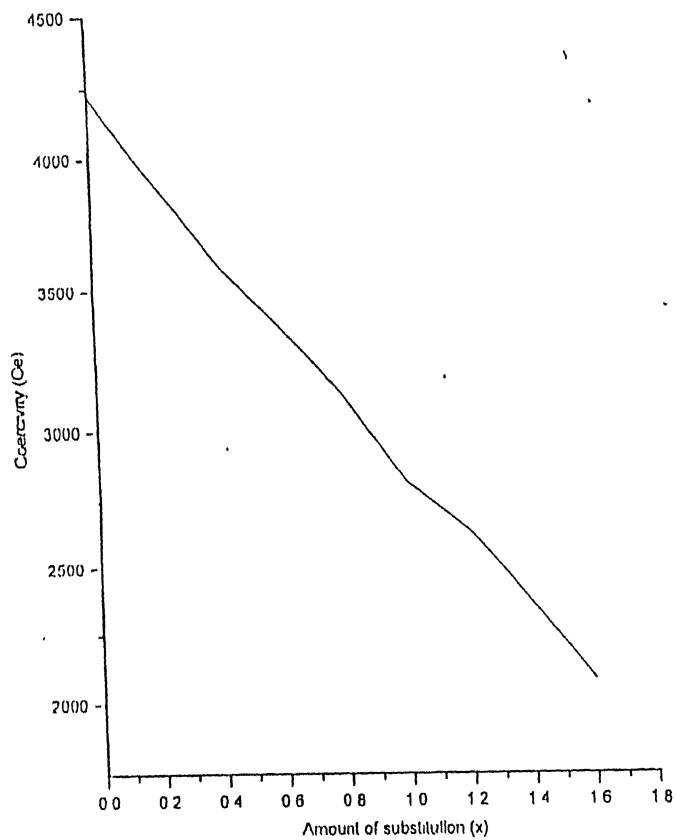


Figure 9 Coercivity for $\text{BaFe}_{12-x}\text{Co}_x\text{O}_{19-2x}$ as a function of x

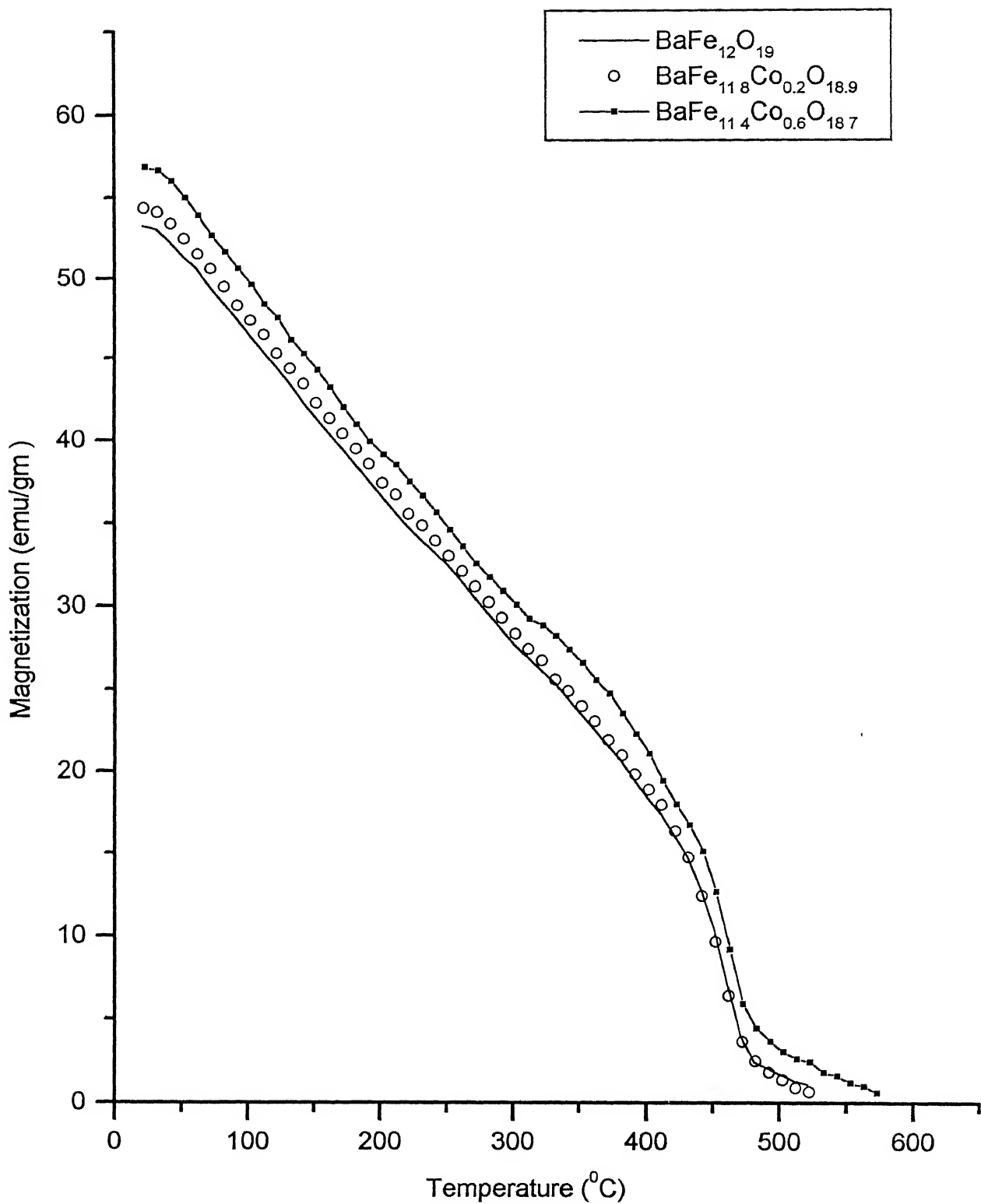


Figure 10 : Variation of magnetization with temperature for cobalt substituted barium ferrite $\text{BaFe}_{12-x}\text{Co}_x\text{O}_{19-x/2}$ ($x=0, 0.2, 0.6$)

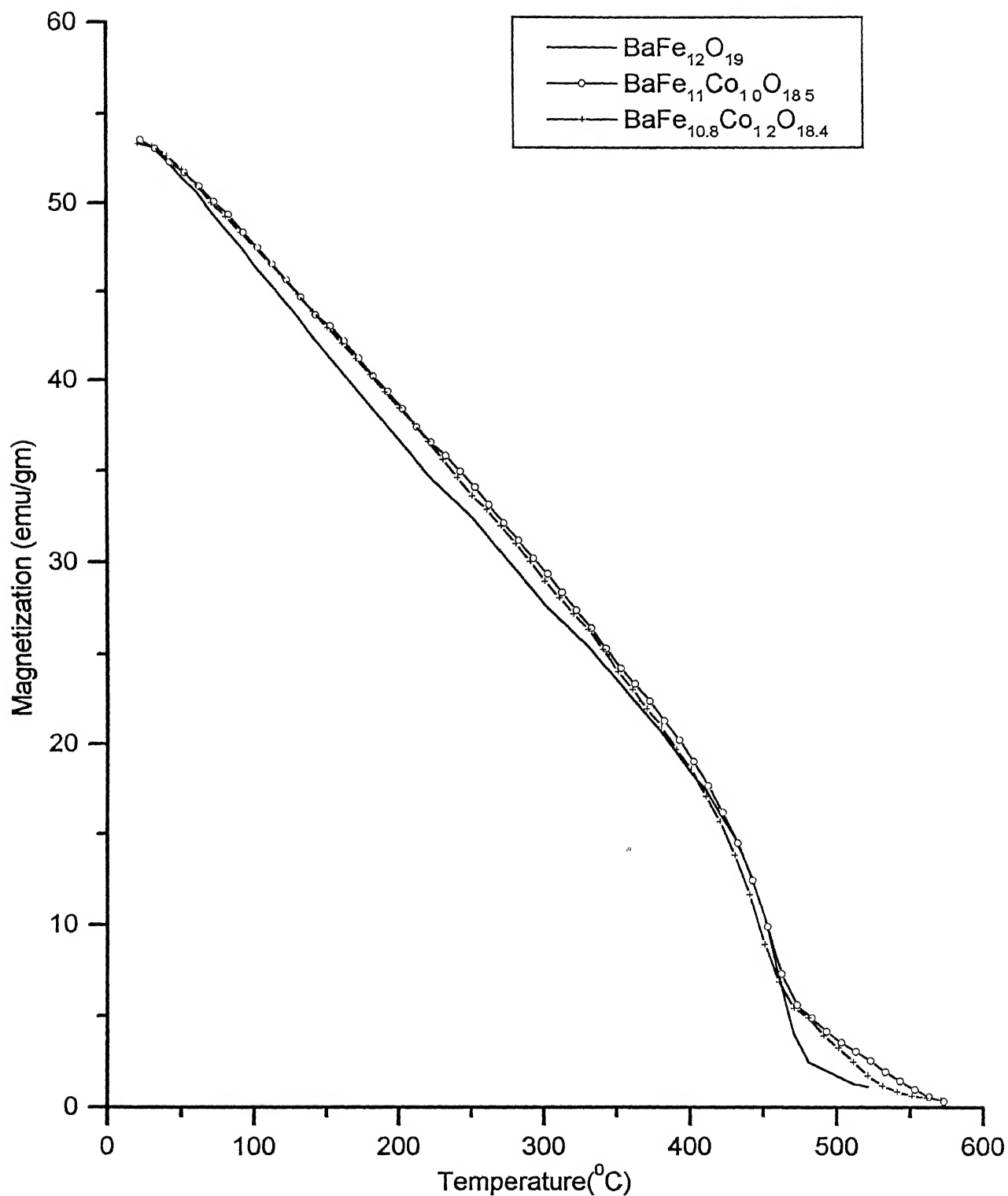


Figure 11 :Magnetization as a function of temperature for pure and cobalt substituted barium ferrite $\text{BaFe}_{12-x}\text{Co}_x\text{O}_{19-x/2}$ ($x=0, 1.0, 1.2$)

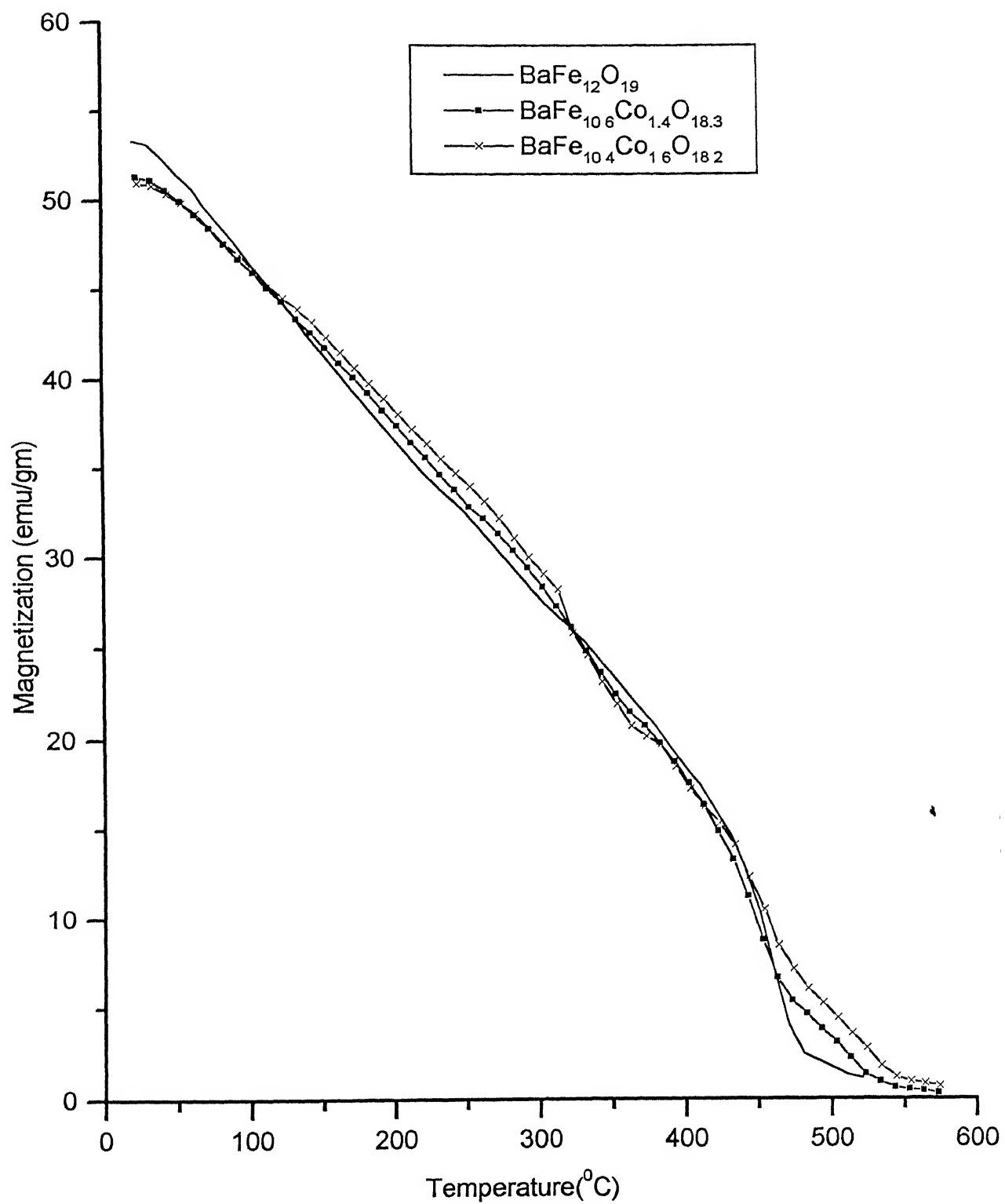


Figure 12 : Magnetization as a function of temperature for pure and cobalt substituted barium ferrite $\text{BaFe}_{12-x}\text{Co}_x\text{O}_{19-x/2}$ ($x=0, 1.4, 1.6$)

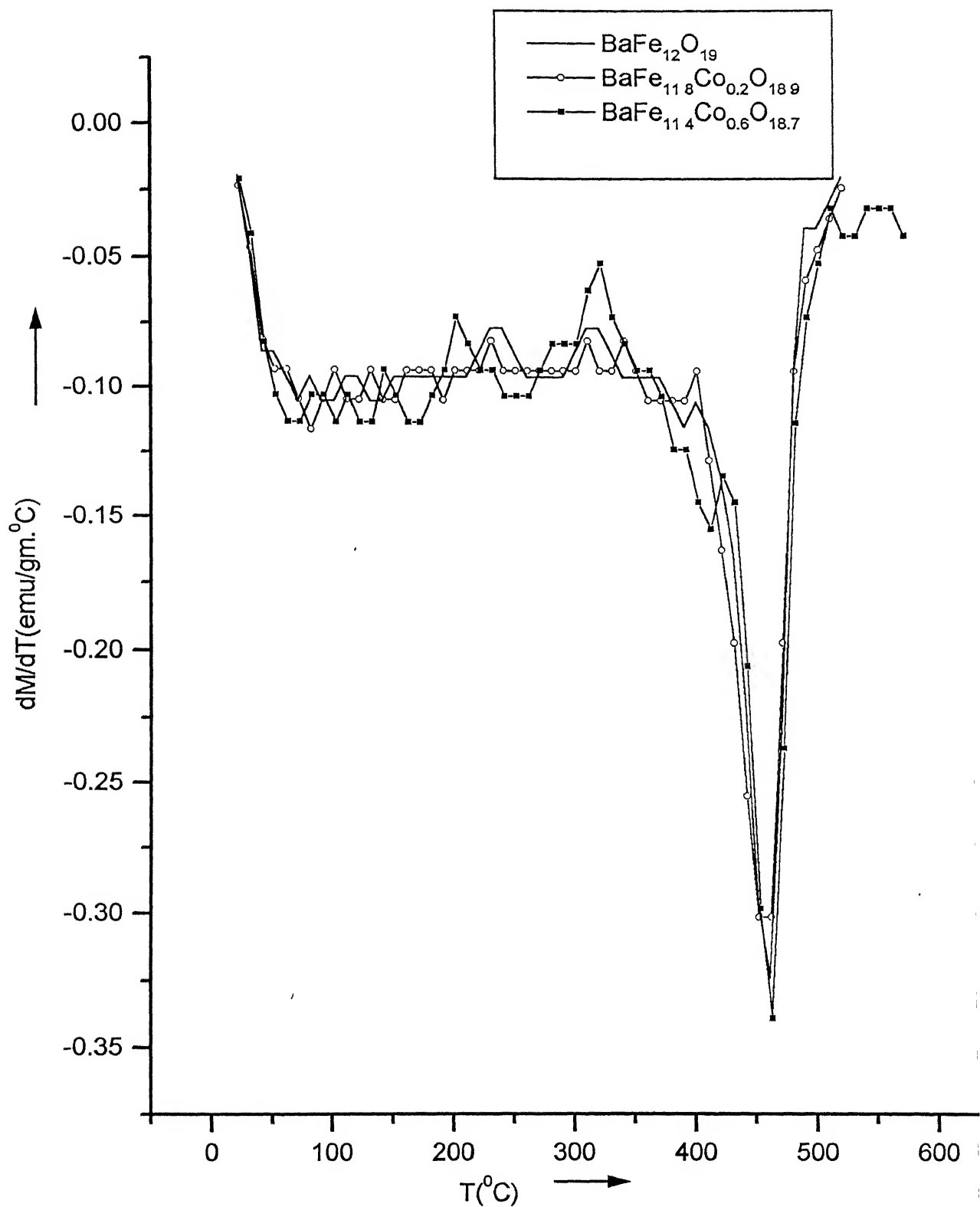


Figure 13 : Variation of $\frac{dM}{dT}$ with temperature for pure and cobalt substituted barium ferrite $\text{BaFe}_{12-x}\text{Co}_x\text{O}_{19-x/2}$ ($x=0, 0.2, 0.6$)

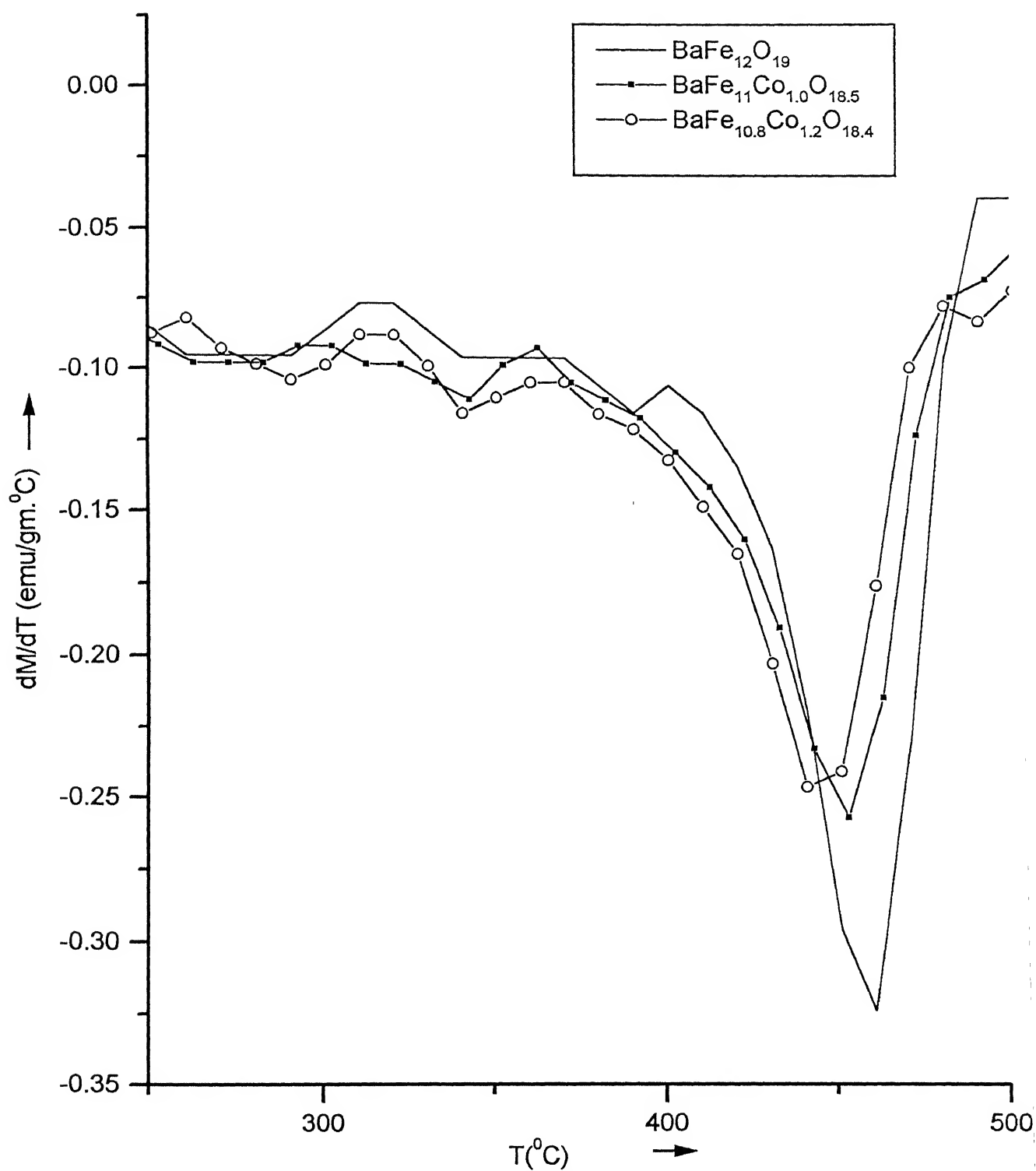


Figure 14 : Variation of dM/dT with temperature pure and cobalt substituted barium ferrite $\text{BaFe}_{12-x}\text{Co}_x\text{O}_{19-x/2}$ ($x=0, 1.0, 1.2$)

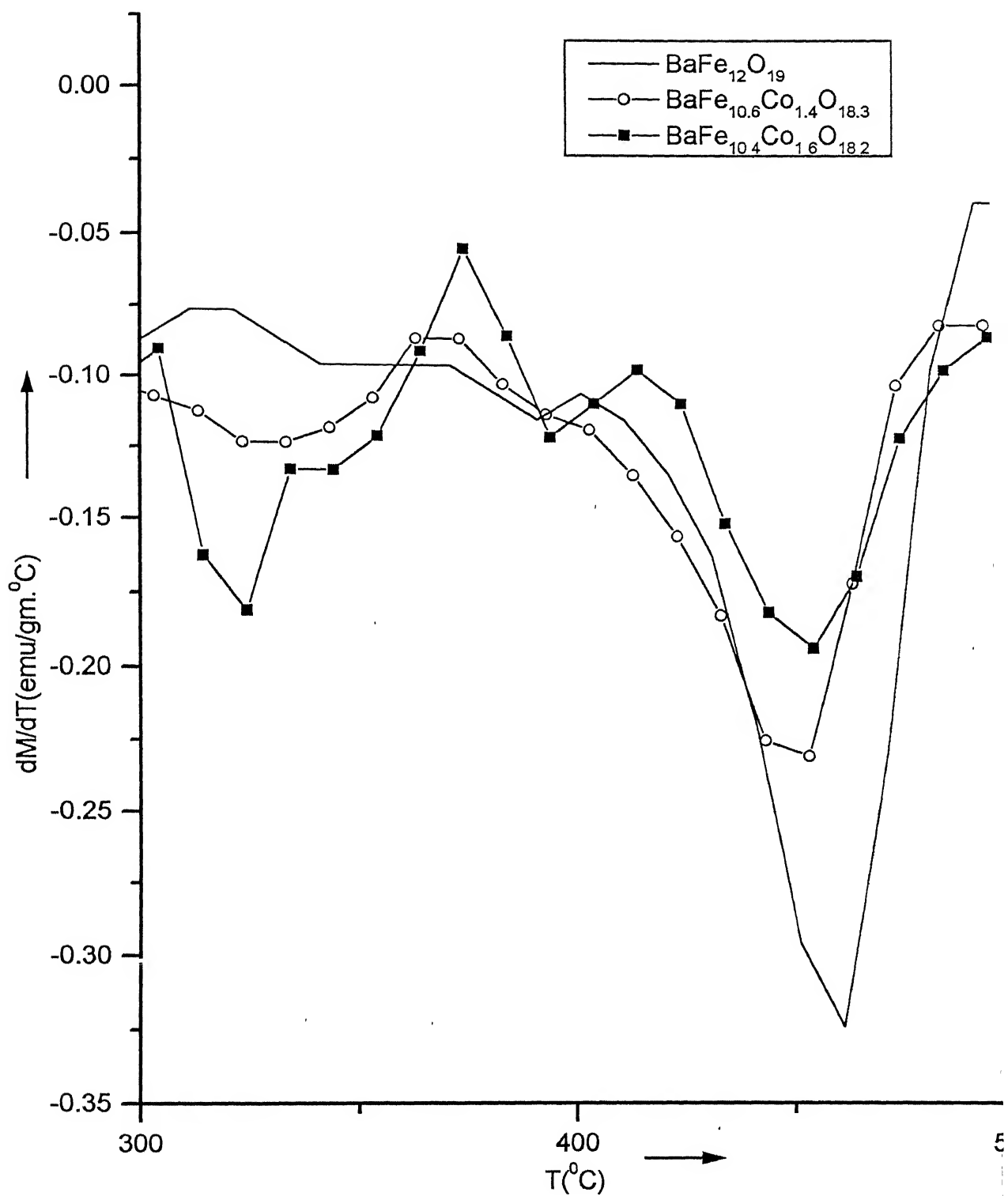


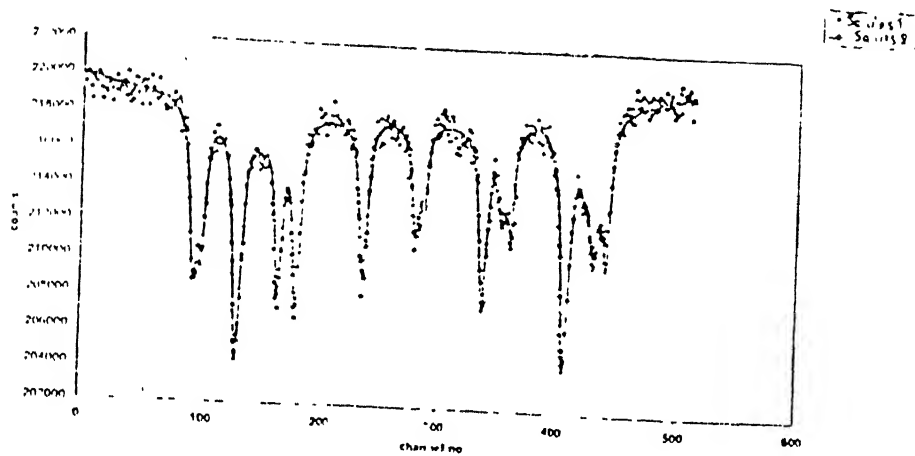
Figure 15 : Variation of dM/dT with temperature for pure and cobalt substituted barium ferrite $\text{BaFe}_{12-x}\text{Co}_x\text{O}_{19-x/2}$ ($x=0, 1.4, 1.6$)

The M_s vs cobalt content graph (Fig., 8) reveals that the saturation magnetization initially increases marginally and assume values within 58-61 emu/gm, for small substitutions, but, decreases beyond $x>1$, (the value for $x=1.6$ being 54.2 emu/gm). However, the coercivity value decreases continuously for all substitutions and correspond to 4223 Oe and 2072 Oe for $x=0$ and $x=1.6$, respectively (Fig., 9). It clearly suggests that cobalt insertion is responsible for the decrease in coercivity values. The magnetization versus temperature (T) curves for samples having cobalt content x varying between zero and 1.6 are shown in Figures 10-12. The corresponding (dM/dT) versus temperature plots are depicted in Figures 13-15. It is observed that with increasing temperature, the magnetization decreases continuously almost at constant rate, up to 450 °C, around the change is somewhat abrupt. This indicates a ferrimagnetic to paramagnetic transition. Also in some cases (e.g., for $x=1.4$ and 1.6), variation of magnetization with temperature contains kinks (Fig., 12), indicative of two-phase behaviour [22]. Nevertheless Curie temperature was determined by the intersection of tangent line at largest slope with flat bottom as per past practice [29]. The values obtained for T_c are given in Table 12. The presence of another phase becomes clear in dM/dT versus temperature plot (Fig., 15) depicting two minima at around 323°C and 460°C while former is associated with the another phase, the latter corresponds to the usual hexa ferrite phase. Looking closely, one notices that the onset of another phase occurs in the samples having $x\sim 1.2$. The new phase could possibly be $Ba_2Co_2Fe_{12}O_{22}$ corresponding to the Curie Temperature 343°C and low saturation magnetization 43 emu/gm [30]. The pellets used for magnetic measurements in fact depicted anisotropic behaviour as magnetization values varied with

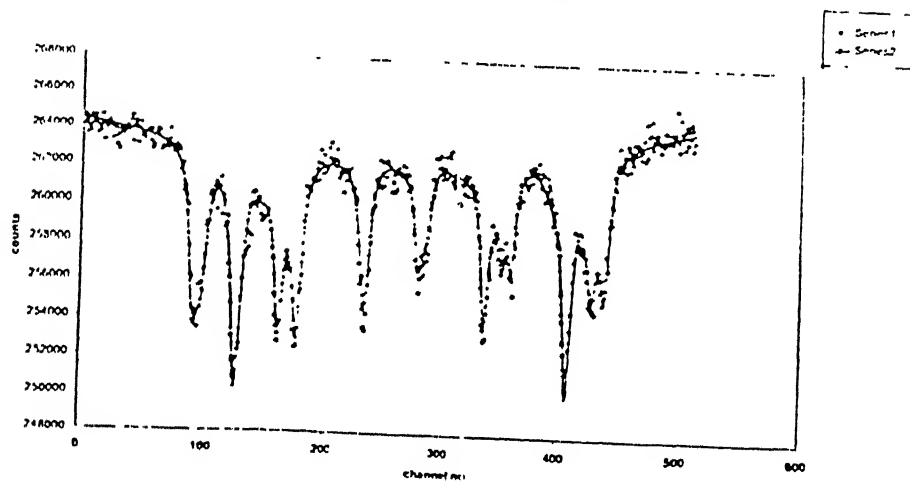
tilt at low fields. This observation provide the existence of preferred orientation which is in conformity with XRD data

3.1.3 MOSSBAUER SPECTROSCOPIC ANALYSIS

Mossbauer spectra of samples containing cobalt recorded at room temperature are shown in Fig., 16-18. These were fitted with sextet sub patterns, corresponding to five different crystallographic sites, $4f_{vi}$, 2a, $4f_{iv}$, 12k and 2b, of pure barium ferrite and a few other locations. The relative spectral areas and corresponding hyper fine fields for six sites are shown in Table 13 .It may be seen that the relative spectral areas of sextets for crystallographic sites $4f_{vi}$, 2a and $4f_{iv}$, are randomly varying with cobalt content and there is no definite trend. However, for relative spectral areas of sextets corresponding to crystallographic sites 12k and 2b are decreasing continuously with cobalt content. It means that cobalt is substituting iron sites at 12k and 2b preferentially, whereas at other sites randomly. The hyperfine fields for all sites except 2b decrease with concentration. In case of 2b site the hyperfine field is not showing any definite trend .The variation is shown in Fig., 19. It is known that uniaxial magneto-crystalline anisotropy in barium ferrite originates largely from occupying bipyramidal 2b and octahedral $4f_{vi}$ sites belonging to R block [24]. This suggest that substitution of these site should decrease anisotropy and hence the coercivity. The decrease of coercivity observed with increase in cobalt content can possibly attributed to preferential filling of 2b site of iron with cob alt. Further, since cobalt ions are occupying both 12k and 2b, sites and irons in these locations exhibit spin upwards, a decrease in saturation magnetization is expected. However, the present result also reveal the development of another phase, it



mossbauer curve for Co doping (0.2)



mossbauer curve for Co doping (x=0.4)

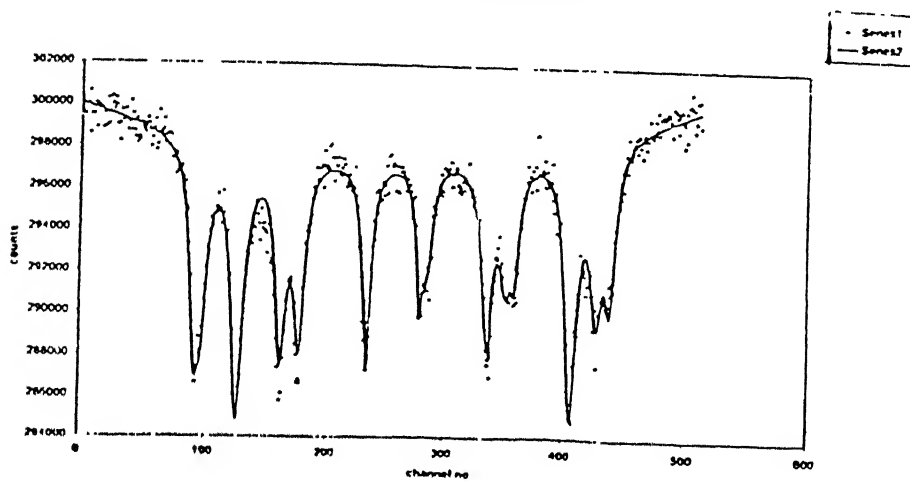


Figure 16 Mossbauer spectra of cobalt substituted barium ferrite $\text{BaFe}_{12-x}\text{Co}_x\text{O}_{19}$ ($x = 0, 0.2, 0.4$).

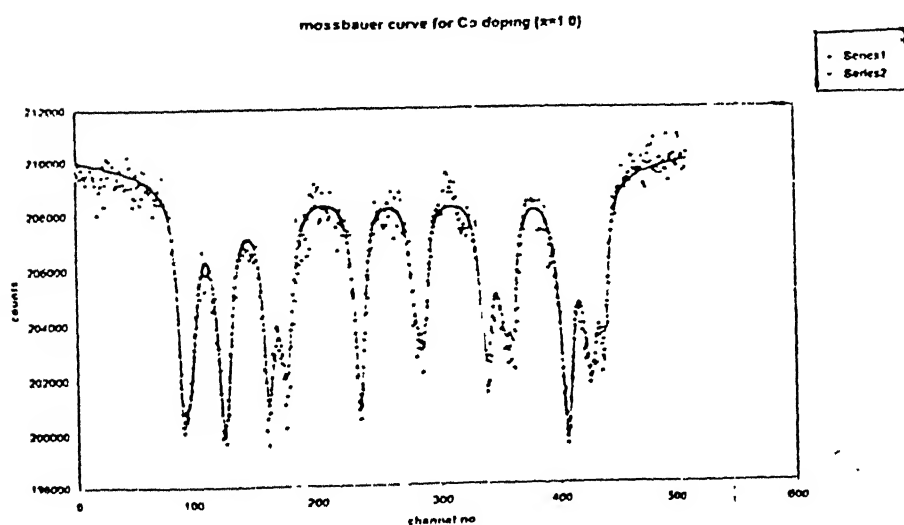
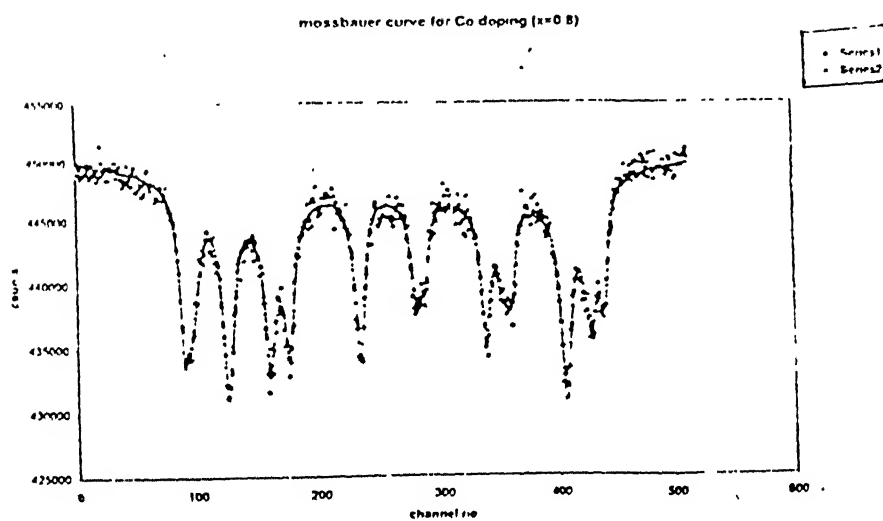
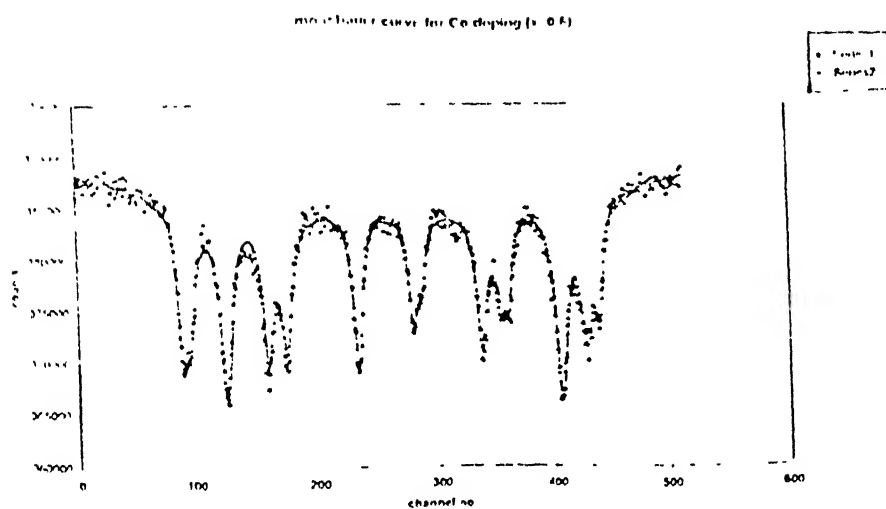


Figure 17 Mossbauer spectra of cobalt substituted barium ferrite $\text{BaFe}_{12-x}\text{Co}_x\text{O}_{19}$ ($x = 0.6, 0.8, 1.0$).

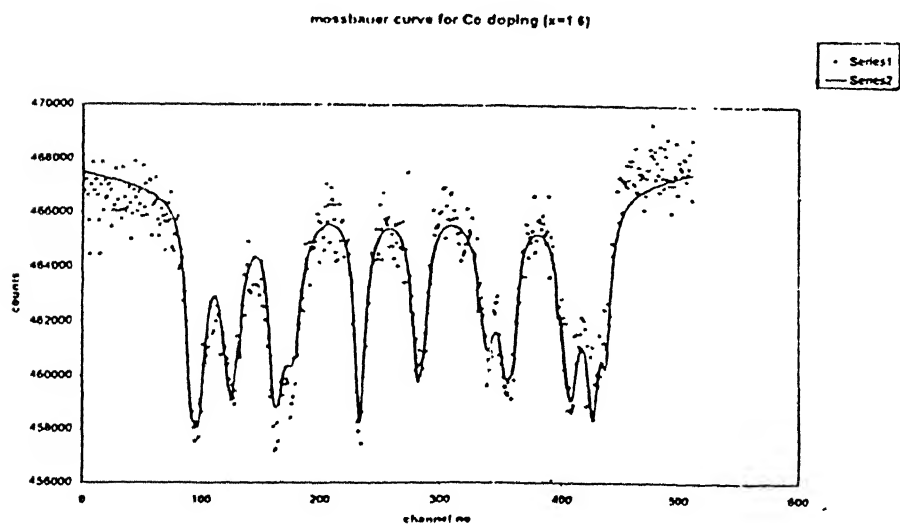
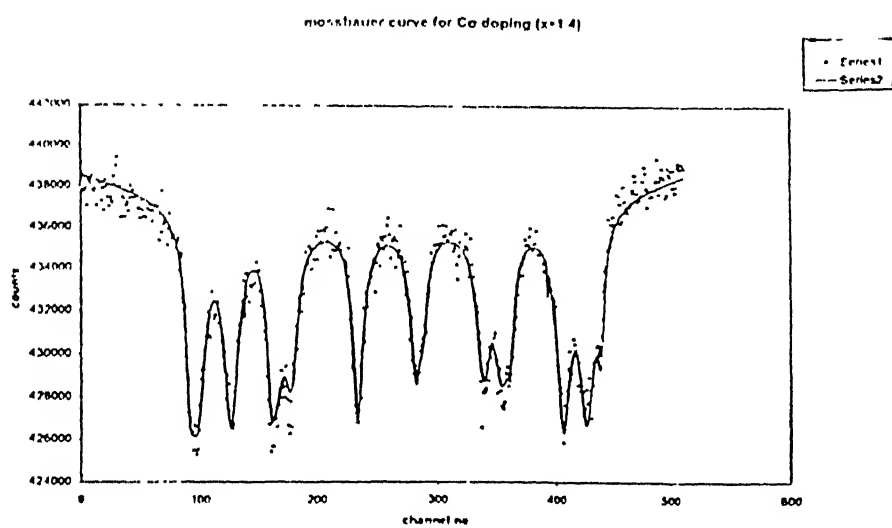
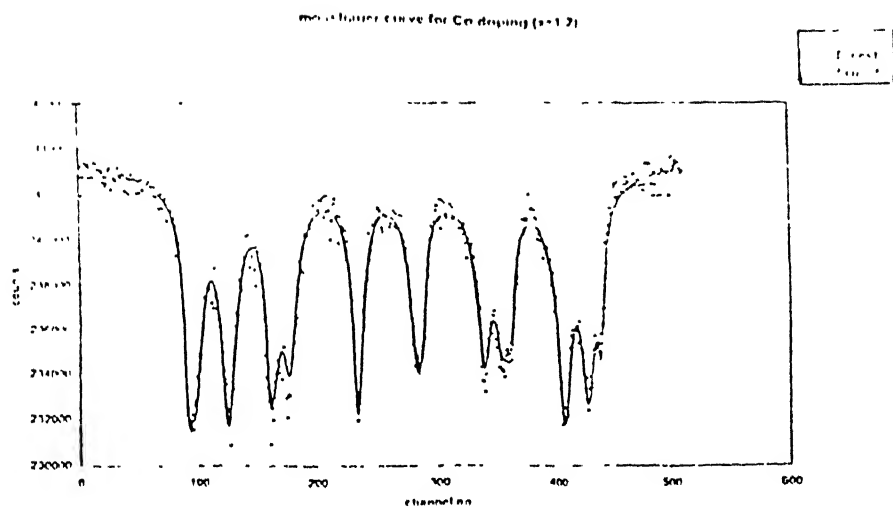


Figure 18. Mossbauer spectra of cobalt substituted barium ferrite $\text{BaFe}_{12-x}\text{Co}_x\text{O}_{19}$ ($x = 1.2, 1.4, 1.6$).

Table 13: Relative spectral areas and hyperfine fields of different crystallographic sites of cobalt containing barium ferrite $\text{BaFe}_{12-x}\text{Co}_x\text{O}_{19-x/2}$

Amount of substitution (x)	Site(4f _v)			Site(2a)			Site(4f _u)			Site(12k)			Site(2b)			Site(new environment)		
	Area (%)	Int. Mag Field (kOe)		Area (%)	Int. Mag Field (kOe)		Area (%)	Int. Mag Field (kOe)		Area (%)	Int. Mag Field (kOe)		Area (%)	Int. Mag Field (kOe)		Area (%)	Int. Mag Field (kOe)	
0.0	8.8	519		11.5	508		25.6	488		47.4	412		7.1	406		-----	-----	
0.2	4.5	522		15.2	509		25.6	487		47.2	413		6.6	407		.99	381	
0.4	14.5	516		3.9	505		29.2	486		41.2	412		9.3	401		1.88	385	
0.6	13.5	512		6.5	501		27.9	483		42.1	410		8.9	400		1.11	390	
0.8	8.8	516		6.3	505		33.3	485		41.7	410		3.0	413		6.8	348	
1.0	7.2	510		9.1	498		34.3	477		43.1	407		3.5	418		2.90	342	
1.2	7.2	510		9.1	499		34.0	476		43.1	407		3.5	417		2.95	342	
1.4	12.2	507		6.6	491		37.0	475		36.6	407		4.1	411		3.5	338	
1.6	16.4	506		10.6	488		23.4	471		38.3	406		4.0	409		7.5	358	

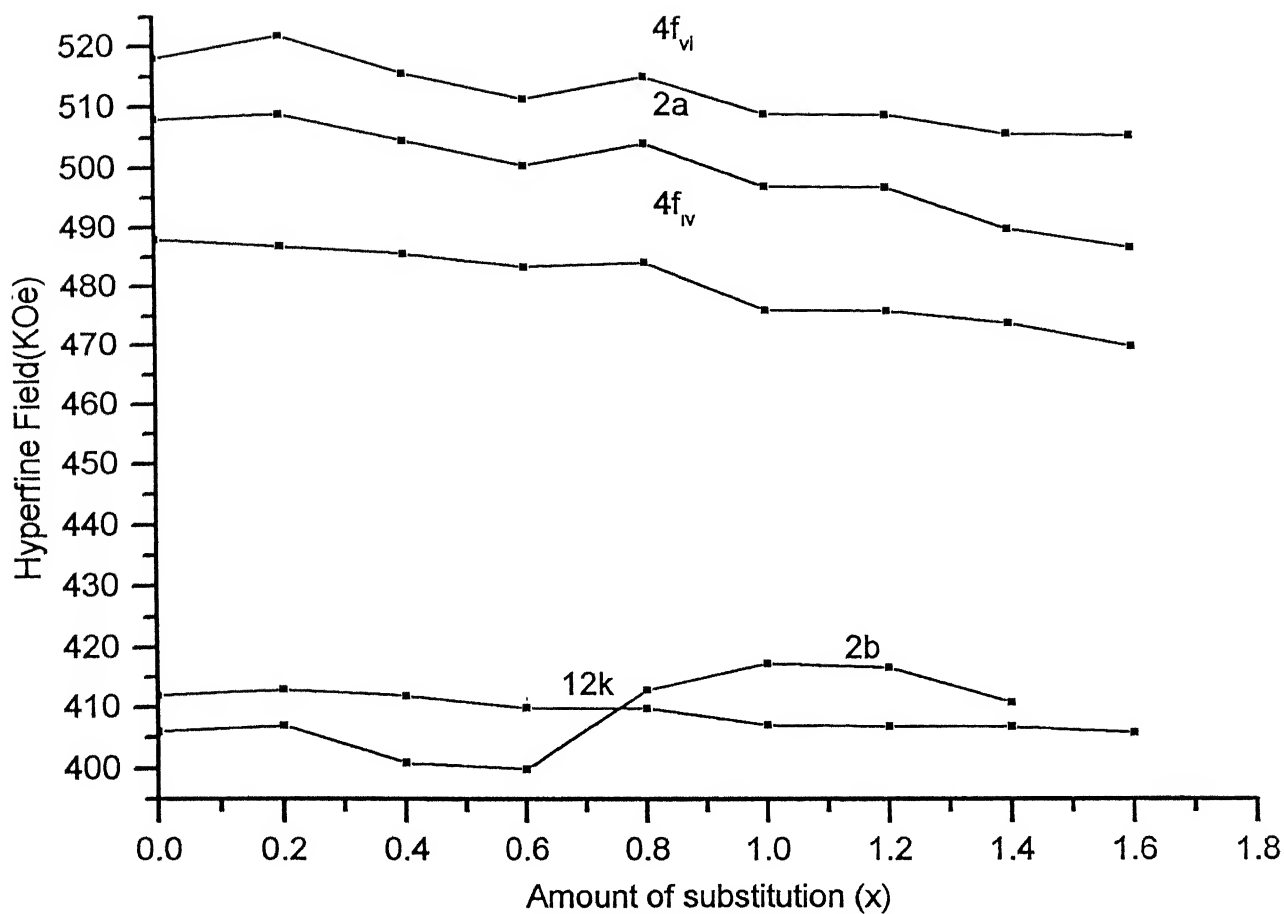


Figure 19 :Variation of hyperfine fields of different sites with cobalt contents in $\text{BaFe}_{12-x}\text{Co}_x\text{O}_{19-x/2}$ ($x=0-1.6$)

Table 20 : Relative spectral areas and hyperfine(Internal magnetic) fields of different crystallographic sites of cobalt and titanium containing barium ferrite $\text{BaFe}_{12-2x}\text{Co}_x\text{Ti}_x\text{O}_{19}$

Amount of substitution (x)	Site(4f _u)		Site(2a)		Site(4f _w)		Site(12k)		Site(2b)		Site(new environment)		Site(new environment)	
	Area (%)	Int. Mag Field (kOe)	Area (%)	Int. Mag Field (kOe)	Area (%)	Int. Mag Field (kOe)	Area (%)	Int. Mag Field (kOe)	Area (%)	Int. Mag Field (kOe)	Area (%)	Int. Mag Field (kOe)	Area (%)	Int. Mag Field (kOe)
0.0	8.7	519	11.5	508	25.3	489	47.4	412	7.1	406.5	-----	-----	-----	-----
0.2	10.5	512	10.4	499	23.4	484	27.1	407	3.5	404	2.2	463	8.6	378
0.4	11.4	507	5.5	494	13.2	481	38.6	409	4.0	416	12.7	461	14.5	352
0.6	6.6	505	11.3	490	23.5	469	28.3	409	1.2	405	6.3	445	22.8	364
0.8	10.9	500	8	481	11.8	470	35.8	404	.2	404	12.2	443	21.1	352
1.0	41	497	4.1	492	14.0	459	20.8	407	6.2	401	1	422	12.9	350

is difficult to a definite picture here. A better correlation may be established between similar experiment are conducted with modified magnetic properties and site occupancy if other ions like nickel and manganese instead of cobalt.

3.2 Co-Ti SUBSTITUTION

When Co^{2+} ions replace Fe^{3+} ions, the charge imbalance may occur or alternatively some oxygen vacancies need to be created. For this reason corresponds are assigned the formula $\text{BaFe}_{12-x}\text{Co}_x\text{O}_{19-x/2}$. In order to maintain charge neutrality two Fe^{3+} ions are substituted with a pair of Co^{2+} and Ti^{4+} to yield products of composition $\text{BaFe}_{12-2x}\text{Co}_x\text{Ti}_x\text{O}_{19}$. As described before, five samples of $\text{BaFe}_{12-2x}\text{Co}_x\text{Ti}_x\text{O}_{19}$ with $x=0.2, 0.4, 0.6, 0.8$ and 1.0 were prepared in present work.

3.2.1 X-RAY ANALYSIS

Their XRD patterns are shown in figures 20-21. The d values and relative intensities of various peaks together with their indices assigned are given in Tables 14-18. For comparison standard data of pure $\text{BaFe}_{12}\text{O}_{19}$ phase are also provided in each case. The results clearly reveal that the sample of $\text{BaFe}_{12-2x}\text{Co}_x\text{Ti}_x\text{O}_{19}$ for all x maintain the hexagonal crystal structure of pure barium ferrite (described in chapter 1). However, increase in cobalt and titanium content, 20.0 diffraction peak becomes gradually strong e.g., the relative intensity of 20.0 peak is 57.45 for samples having x equal to 1.0. Also, while diffraction peaks 20.5 is always strong, 11.0 exhibit

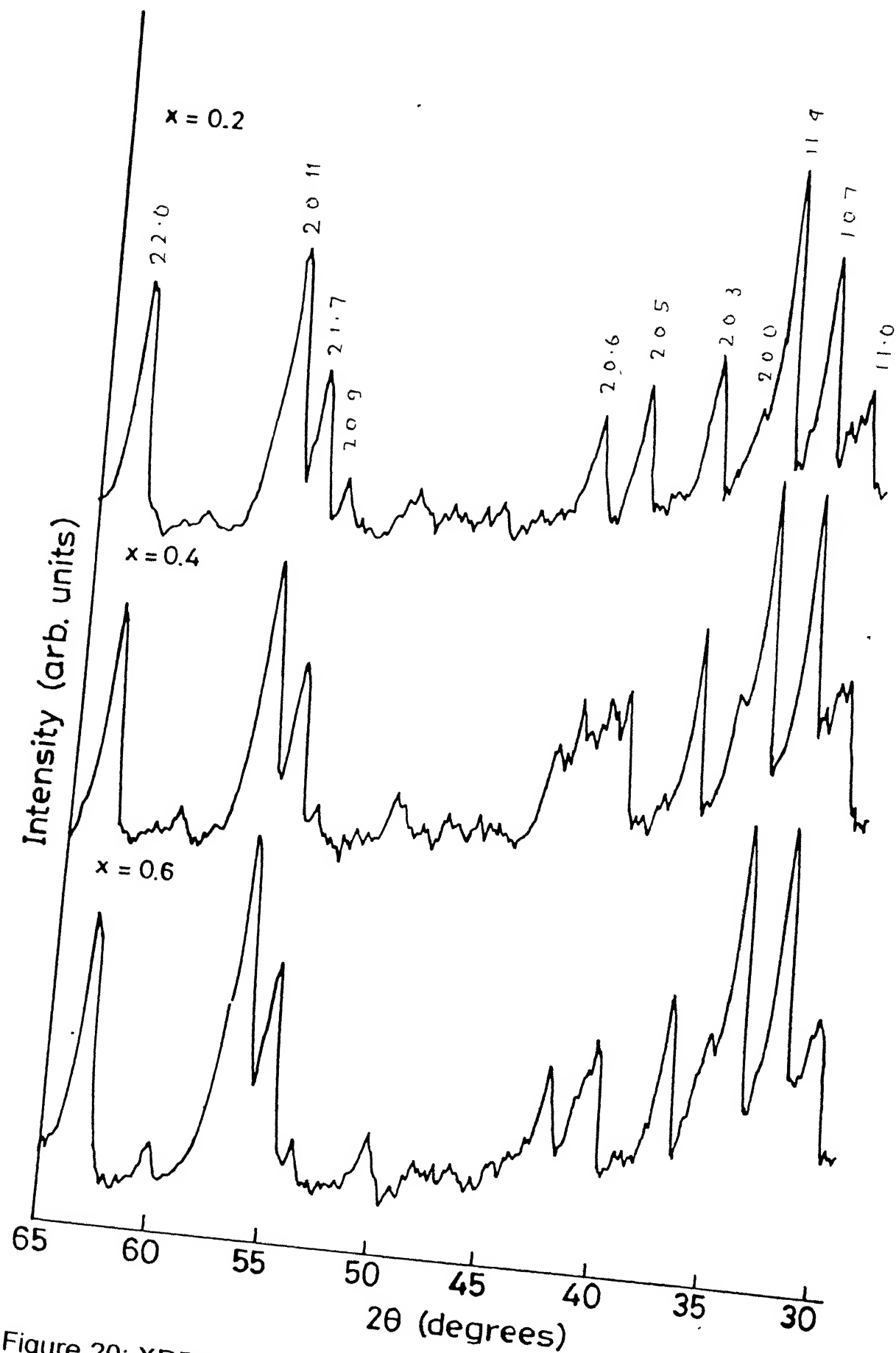


Figure 20: XRD pattern of cobalt and titanium substituted barium ferrite $\text{BaFe}_{12-2x}\text{Co}_x\text{Ti}_x\text{O}_{19}$ ($x=0.2, 0.4$ and 0.6)

CENTRAL LIBRARY
I. I. T., KANPUR

No. A 130435

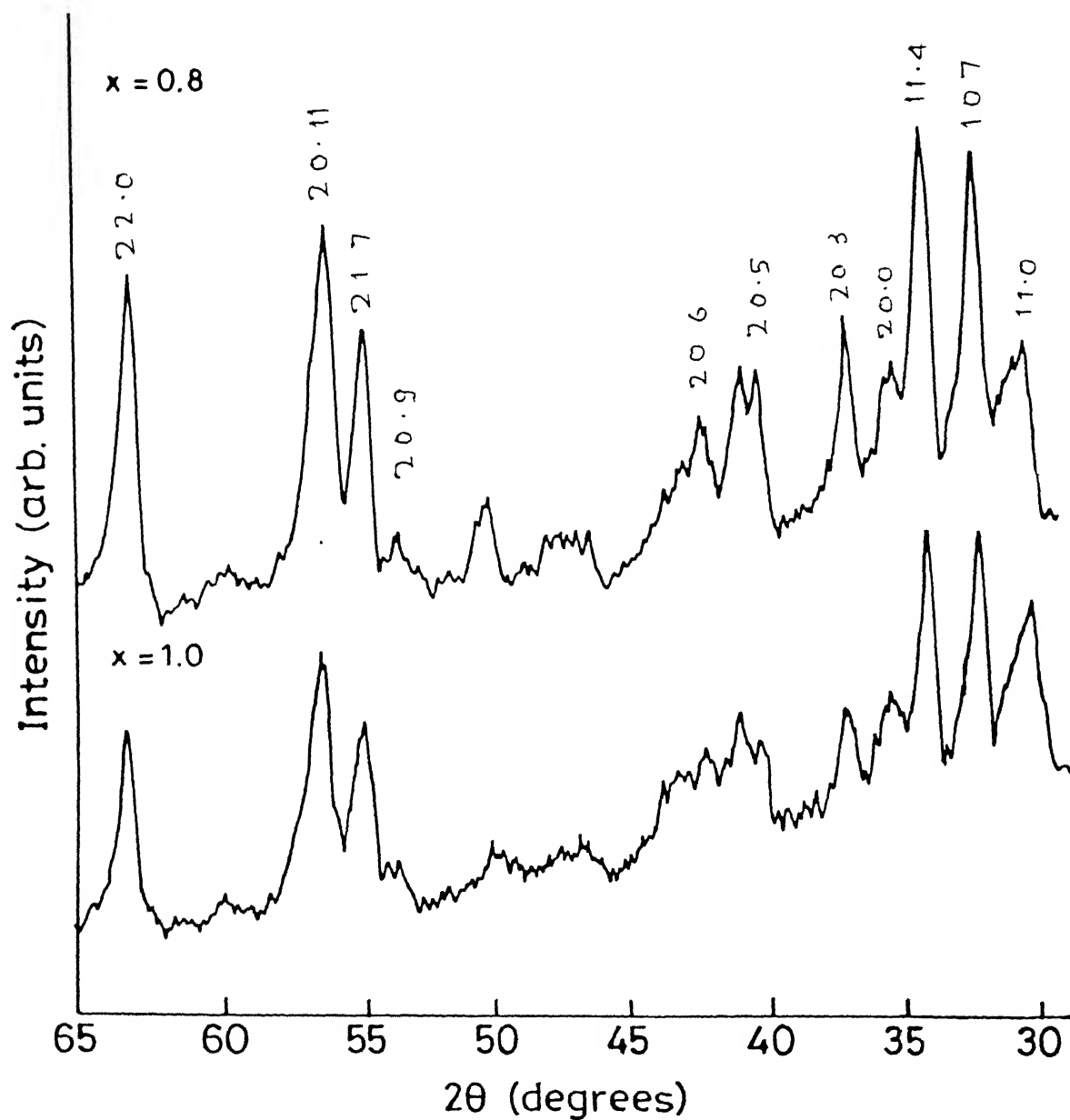


Figure 21: XRD pattern of cobalt and titanium substituted barium ferrite $\text{BaFe}_{12-2x}\text{Co}_x\text{Ti}_x\text{O}_{19}$ ($x=0.8$ and 1.0)

Table 14: Interplanar spacings and intensities of various peaks observed in XRD of cobalt and titanium substituted barium ferrite $\text{BaFe}_{12-2x}\text{Co}_x\text{Ti}_x\text{O}_{19}$ ($x=0.2$)

d-values for $\text{BaFe}_{12}\text{O}_{19}$ ($^{\circ}\text{\AA}$)	Interplanar spacings observed for $\text{BaFe}_{12-2x}\text{Co}_x\text{Ti}_x\text{O}_{19}$ ($x=0.2$)	Intensities for $\text{BaFe}_{12}\text{O}_{19}$	Intensities observed for $\text{BaFe}_{12-2x}\text{Co}_x\text{Ti}_x\text{O}_{19}$ ($x=0.2$)	hk.l indices
2.94	2.93	55	44.42	1 1 . 0
2.78	2.77	100	78.31	1 0 . 7
2.62	2.61	98	100	1 1 . 4
2.55	2.54	11	37.34	2 0 . 0
2.42	2.41	60	50.30	2 0 . 3
2.23	2.22	29	40.00	2 0 . 5
2.13	2.13	18	31.17	2 0 . 6
1.81	1.81	10	7.23	2 0 . 9
1.66	1.66	53	36.29	2 1 . 7
1.63,1.62, 1.61	1.62	30,58,10	66.86	2 0 . 11
1.47	1.47	63	55.12	2 2 2 . 0

The standard data for pure $\text{BaFe}_{12}\text{O}_{19}$ is given for the sake of comparison.

Table 15 : Interplanar spacings and intensities of various peaks observed in XRD of cobalt and titanium substituted barium ferrite $\text{BaFe}_{12-2x}\text{Co}_x\text{Ti}_x\text{O}_{19}$ ($x=0.4$)

d-values for $\text{BaFe}_{12}\text{O}_{19}$ ($^{\circ}\text{\AA}$)	Interplanar spacings observed for $\text{BaFe}_{12-2x}\text{Co}_x\text{Ti}_x\text{O}_{19}$ ($x=0.4$)	Intensities for $\text{BaFe}_{12}\text{O}_{19}$	Intensities observed for $\text{BaFe}_{12-2x}\text{Co}_x\text{Ti}_x\text{O}_{19}$ ($x=0.4$)	hk.l indices
2.94	2.94	55	52.77	1 1 . 0
2.78	2.77	100	97.77	1 0 . 7
2.62	2.62	98	100	1 1 . 4
2.55	2.55	11	47.5	2 0 . 0
2.42	2.42	60	63.05	2 0 . 3
2.23	2.23	29	46.11	2 0 . 5
2.13	2.13	18	42.77	2 0 . 6
1.81	1.81	10	16.94	2 0 . 9
1.66	1.66	53	45.69	2 1 . 7
1.63,1.62, 1.61	1.62	30,58,10	70	2 0 . 11
1.47	1.47	63	56.11	2 2 . 0

The standard data for pure $\text{BaFe}_{12}\text{O}_{19}$ is given for the sake of comparison.

Table 16: Interplanar spacings and intensities of various peaks observed in XRD of cobalt and titanium substituted barium ferrite $\text{BaFe}_{12-2x}\text{Co}_x\text{Ti}_x\text{O}_{19}$ ($x=0.6$)

d-values for $\text{BaFe}_{12}\text{O}_{19}$ ($^{\circ}\text{\AA}$)	Interplanar spacings observed for $\text{BaFe}_{12-2x}\text{Co}_x\text{Ti}_x\text{O}_{19}$ ($x=0.6$)	Intensities for $\text{BaFe}_{12}\text{O}_{19}$	Intensities observed for $\text{BaFe}_{12-2x}\text{Co}_x\text{Ti}_x\text{O}_{19}$ ($x=0.6$)	hkl indices
2.94	2.94	55	53.86	1 1 0
2.78	2.77	100	100	1 0 7
2.62	2.61	98	99.28	1 1 4
2.55	2.54	11	45.41	2 0 0
2.42	2.42	60	55.01	2 0 3
2.23	2.23	29	39.54	2 0 5
2.13	2.13	18	34.38	2 0 6
1.81	1.81	10	13.03	2 0 9
1.66	1.66	53	53.86	2 1 7
1.63, 1.62, 1.61	1.62	30, 58, 10	83.66	2 0 11
1.47	1.47	63	63.32	2 2 0

The standard data for pure $\text{BaFe}_{12}\text{O}_{19}$ is given for the sake of comparison.

Table 17: Interplanar spacings and intensities of various peaks observed in XRD of cobalt and titanium substituted barium ferrite, $\text{BaFe}_{12-2x}\text{Co}_x\text{Ti}_x\text{O}_{19}$ ($x=0.8$)

d-values for $\text{BaFe}_{12}\text{O}_{19}$ ($^{\circ}\text{\AA}$)	Interplanar spacings observed for $\text{BaFe}_{12-2x}\text{Co}_x\text{Ti}_x\text{O}_{19}$ ($x=0.8$)	Intensities for $\text{BaFe}_{12}\text{O}_{19}$	Intensities observed for $\text{BaFe}_{12-2x}\text{Co}_x\text{Ti}_x\text{O}_{19}$ ($x=0.8$)	hkl indices
2.94	2.93	55	52.92	1 1 . 0
2.78	2.77	100	94.76	1 0 . 7
2.62	2.62	98	100	1 1 . 4
2.55	2.53	11	47.69	2 0 . 0
2.42	2.41	60	59.07	2 0 . 3
2.23	2.23	29	46.46	2 0 . 5
2.13	2.13	18	36.30	2 0 . 6
1.81	1.81	10	18.46	2 0 . 9
1.66	1.66	53	58.46	2 1 . 7
1.63,1.62, 1.61	1.62	30,58,10	80	2 0 . 11
1.47	1.47	63	69.23	2 2 . 0

The standard data for pure $\text{BaFe}_{12}\text{O}_{19}$ is given for the sake of comparison.

Table 18: Interplanar spacings and intensities of various peaks observed in XRD of cobalt and titanium substituted barium ferrite $\text{BaFe}_{12-2x}\text{Co}_x\text{Ti}_x\text{O}_{19}$ ($x=1.0$)

d-values for $\text{BaFe}_{12}\text{O}_{19}$ ($^{\circ}\text{\AA}$)	Interplanar spacings observed for $\text{BaFe}_{12-2x}\text{Co}_x\text{Ti}_x\text{O}_{19}$ ($x=1.0$)	Intensities for $\text{BaFe}_{12}\text{O}_{19}$	Intensities observed for $\text{BaFe}_{12-2x}\text{Co}_x\text{Ti}_x\text{O}_{19}$ ($x=1.0$)	hkl indices
2.94	2.95	55	80.88	1 1 . 0
2.78	2.78	100	97.05	1 0 . 7
2.62	2.62	98	100	1 1 . 4
2.55	2.52	11	57.35	2 0 . 0
2.42	2.41	60	52.94	2 0 . 3
2.23	2.23	29	45.58	2 0 . 5
2.13	2.13	18	43.38	2 0 . 6
1.81	1.81	10	19.66	2 0 . 9
1.66	1.66	53	51.47	2 1 . 7
1.63,1.62, 1.61	1.62	30,58,10	67.64	2 0 . 11
1.47	1.47	63	50.00	2 2 . 0

The standard data for pure $\text{BaFe}_{12}\text{O}_{19}$ is given for the sake of comparison.

high intensity in samples corresponding to $x=1.0$. The relative intensity data reveal some preferred orientation (i.e., textured nature) of cobalt and titanium containing barium ferrite phase.

3.2.2 MAGNETIC MEASUREMENTS

The magnetization versus applied field curve of cobalt-titanium substituted barium ferrite for $x = 0.2, 0.4, 0.6, 0.8$ and 1.0 are shown in Figure 22. The M_s Vs x plot (Fig.,23) depicts that the saturation magnetization is marginally affected. It increases a little for small x 's, but, decreases with increase in level of substitution. The variation of coercivity as a function of cobalt content (x) is shown in Figure 24. It depicts that the coercivity H_c , drops drastically from 4223 Oe to 407 Oe as x increases from $x = 0$ to 1.0 . Also, decrease seems to be exponential in nature and follow the equation

$H_c = H_{c0} \exp(-\alpha x)$ where H_{c0} is the coercivity value for $x=0$ and α is a constant. The coercivity and saturation magnetization data of Co-Ti substituted barium ferrite $BaFe_{12-2x}Co_xTi_xO_{19}$ are given in Table 19.

Table 19: Saturation Magnetization and Coercivity of different cobalt and titanium containing barium ferrite $BaFe_{12-2x}Co_xTi_xO_{19}$

Amount of substitution x	Saturation Magnetization (emu/gm)	Coercivity (Oe)	Curie Temperature(a) ($^{\circ}C$)	Curie Temperature(b) ($^{\circ}C$)
0.0	58.8	4223	481.3	460.4
0.2	61.2	2676	-----	-----
0.4	61.1	1600	448.5	388.4
0.6	60.5	1110	430.5	383.2
0.8	58.8	786	-----	-----
1.0	56.2	407	392.4	362.7

a) Intersection of tangent at largest slope with X-axis

b) Minima of dM/dT vs Temperature plots

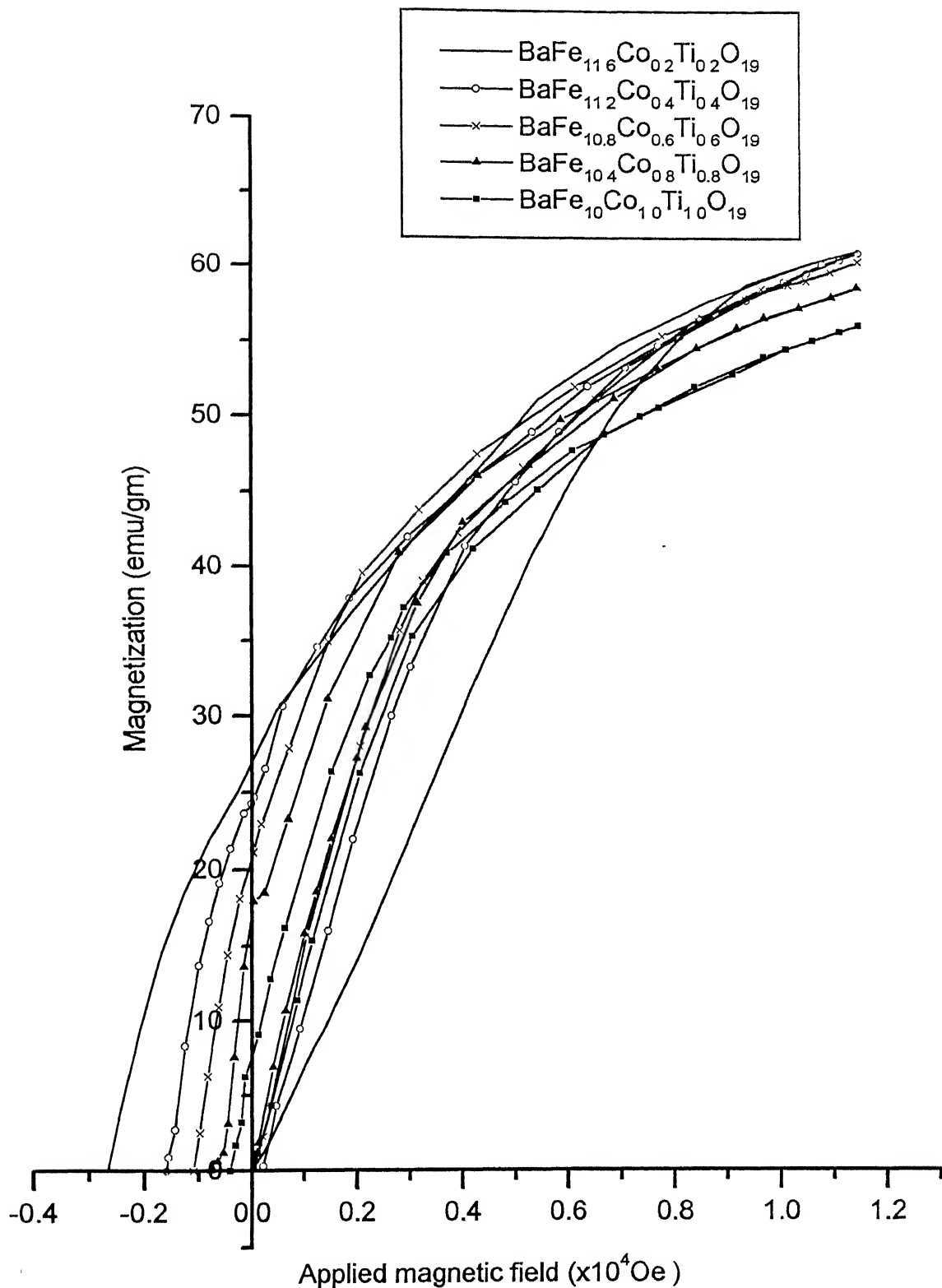


Figure 22 : Magnetization versus applied field curve for Cobalt and Titanium substituted barium ferrite $\text{BaFe}_{12-2x}\text{Co}_x\text{Ti}_x\text{O}_{19}$ ($x = 0.2, 0.4, 0.6, 0.8, 1.0$)

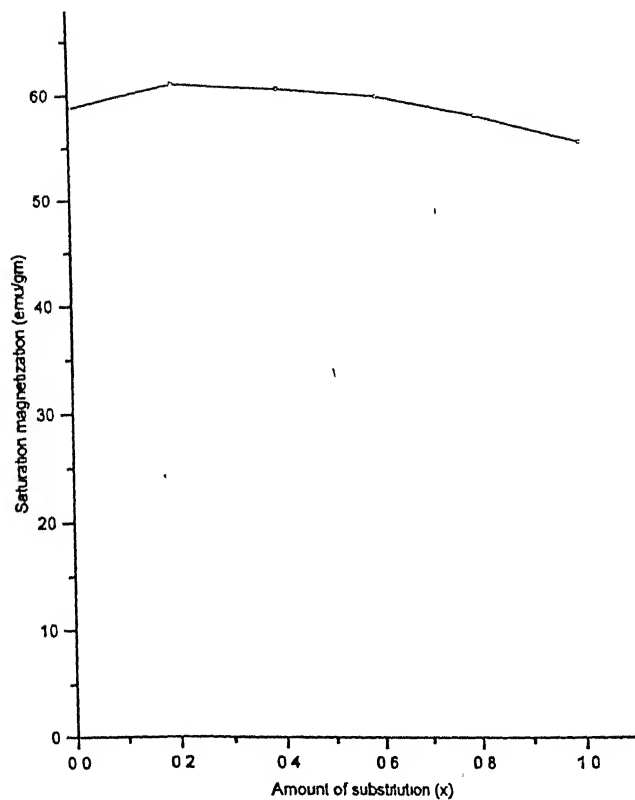


Figure 23 : Saturation magnetization for $\text{BaFe}_{12-2x}\text{Co}_x\text{Ti}_x\text{O}_{10}$ as a function of substitution x

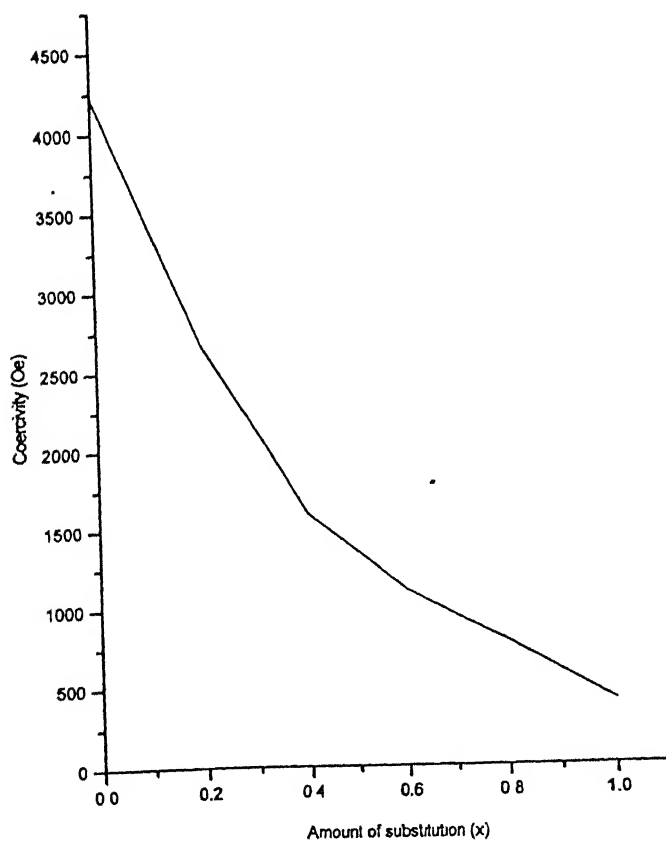


Figure 24 Coercivity for $\text{BaFe}_{12-2x}\text{Co}_x\text{Ti}_x\text{O}_{10}$ as a function of x

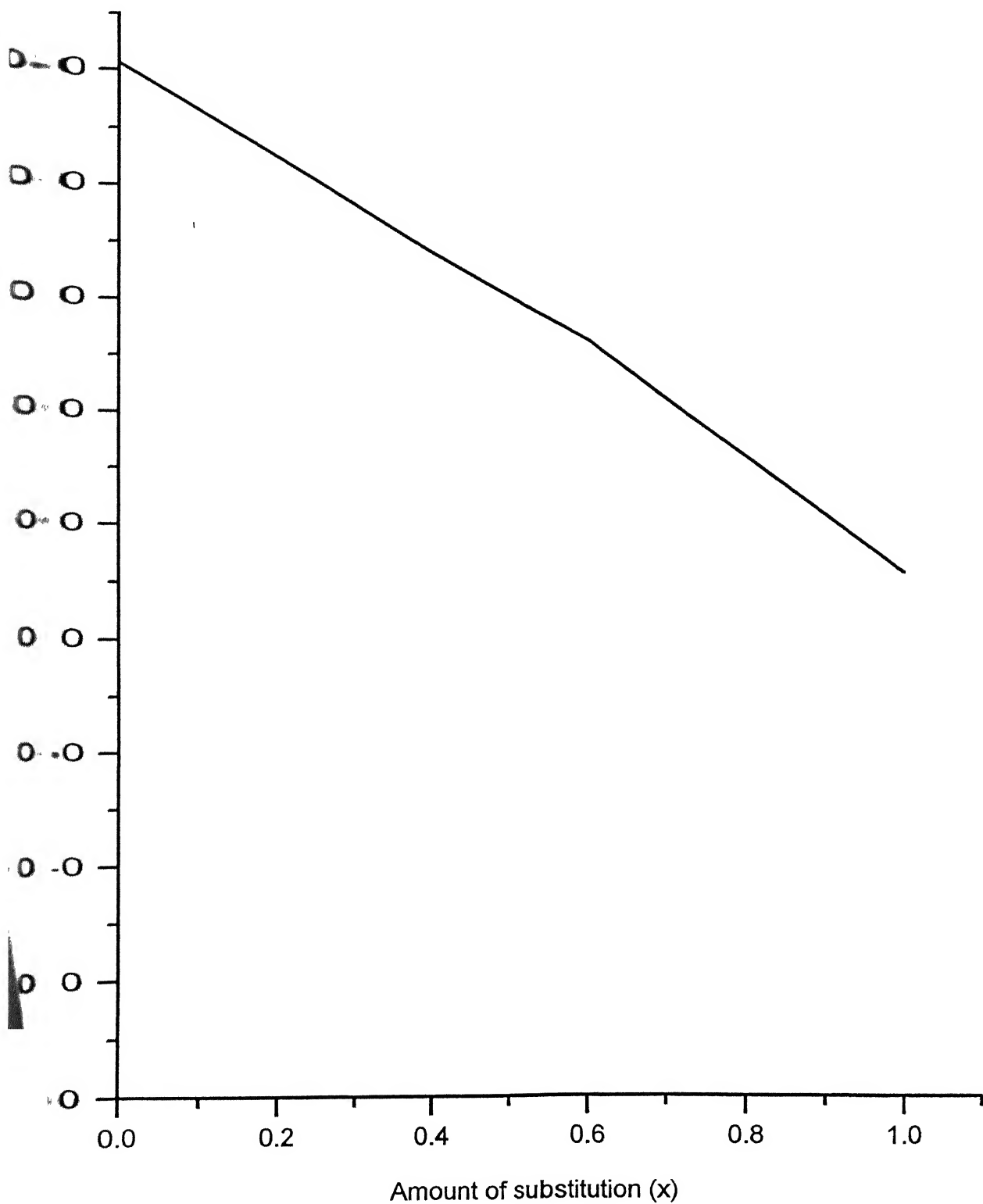


Figure 25 :Curie temperature for $\text{BaFe}_{12-2x}\text{Co}_x\text{Ti}_x\text{O}_{19}$ as a fuction of substitution x

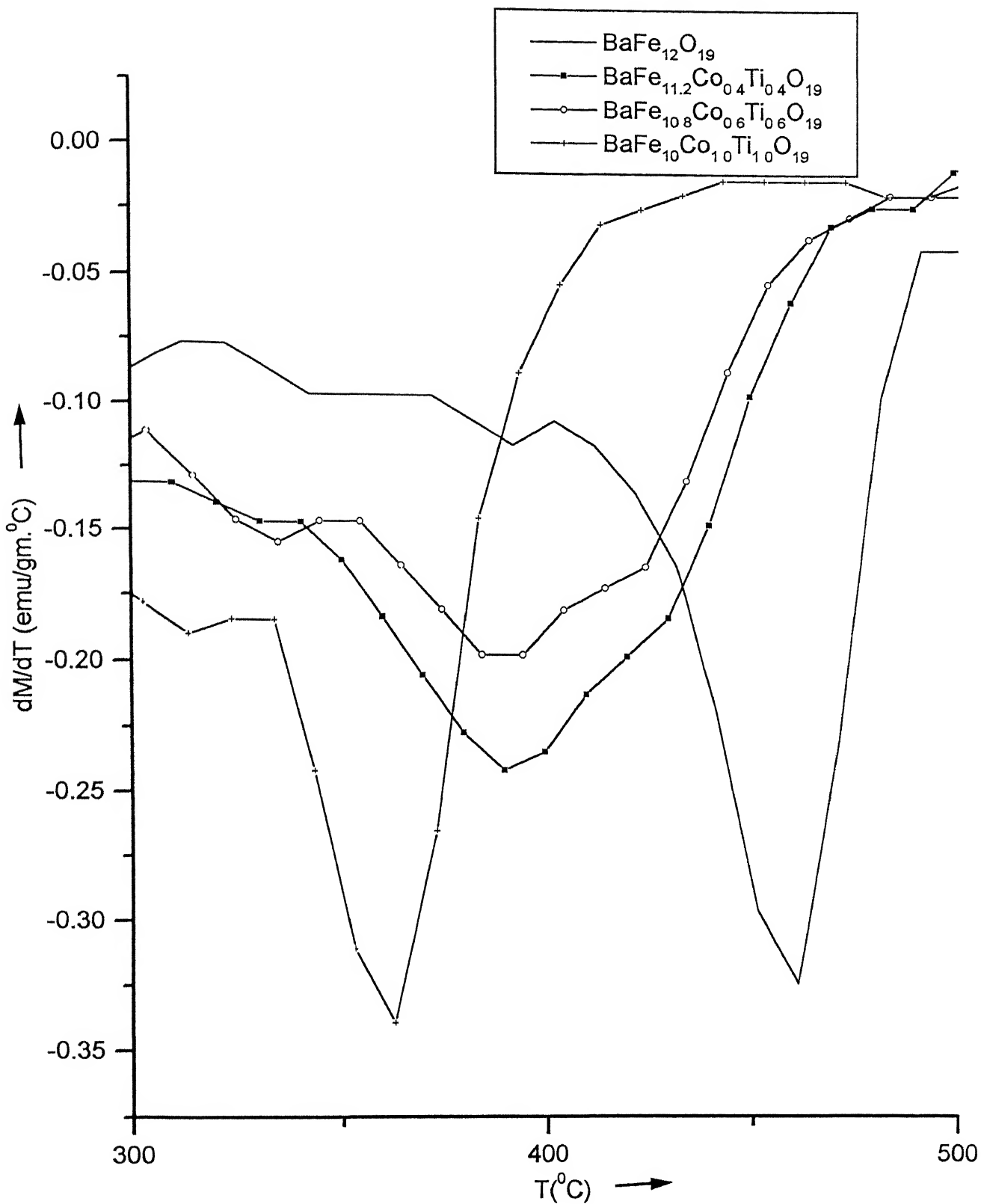


Figure 27 : Variation of dM/dT with Temperature for Cobalt and Titanium substituted barium ferrite $\text{BaFe}_{12-2x}\text{Co}_x\text{Ti}_x\text{O}_{19}$ ($x = 0, 0.4, 0.6, 1.0$)

The magnetization versus Temperature (T) and dM/dT vs T plots for $x = 0, 0.4, 0.6$ and 1.0 are shown in Figure 25-26. These clearly indicate that onset of paramagnetism occur at lower temperatures with increased amount of Co-Ti substitution as determined by interaction of tangent line at largest slope with flat bottom. The Curie temperature (T_c) as a function of amount of Co-Ti substitution (x) is shown in Figure 27. and values are given in Table 8819. Co^{2+} and Ti^{4+} insertion is expected to weaken the exchange interaction between iron ions, in turn, cause reduction in Curie temperature [31].

3.2.3 MOSSBAUER SPECTROSCOPIC ANALYSIS

Typical Mossbauer spectra for samples with $x = 0.2, 0.4, 0.6, 0.8$ and 1.0 at room temperature are shown in the Figures 28-29. These were fitted with various sextet subpatterns corresponding to five different crystallographic iron sites $4f_{iv}$, $4f_{vi}$, $2a$, $2b$ and $12k$ of pure barium ferrite and others possibly arisen because of Co-Ti substitution. The relative spectral areas and hyperfine fields for each to different site are given in Table 20. The relative spectral areas of sextets corresponding crystallographic sites $12k$, $2b$ and $4f_{iv}$ decrease whereas for $4f_{vi}$ and $2a$ sites remains more or less constant with increase in Co-Ti substitution. The hyperfine field for different crystallographic sites as a function of amount of Co-Ti substitution is shown in Figure 30. Notice that these values for sites $4f_{vi}$, $2a$ and $4f_{iv}$ decrease with

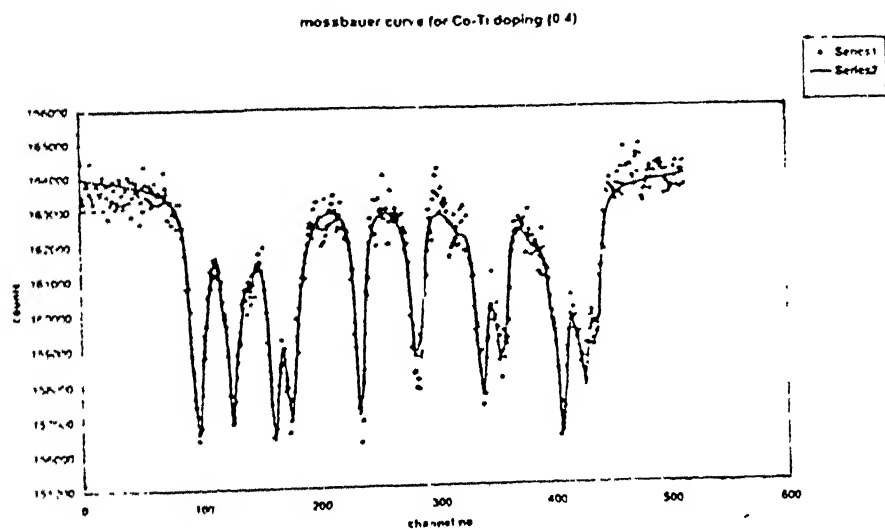
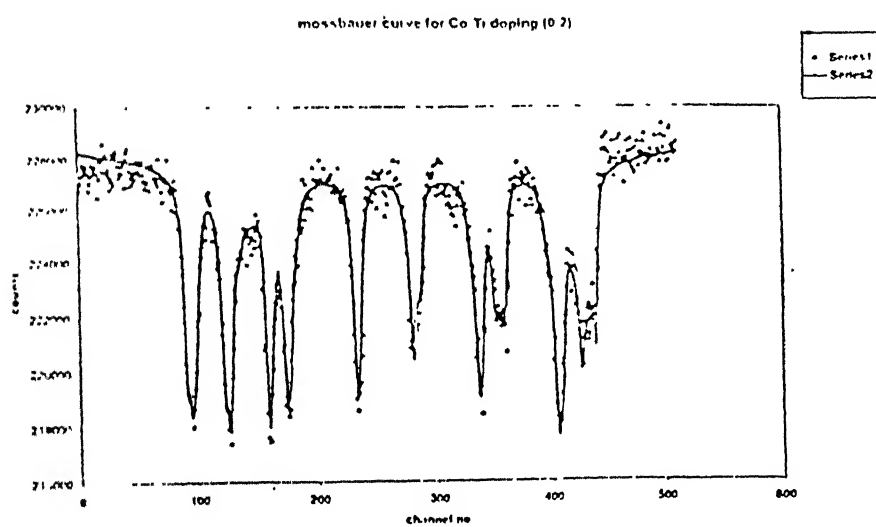
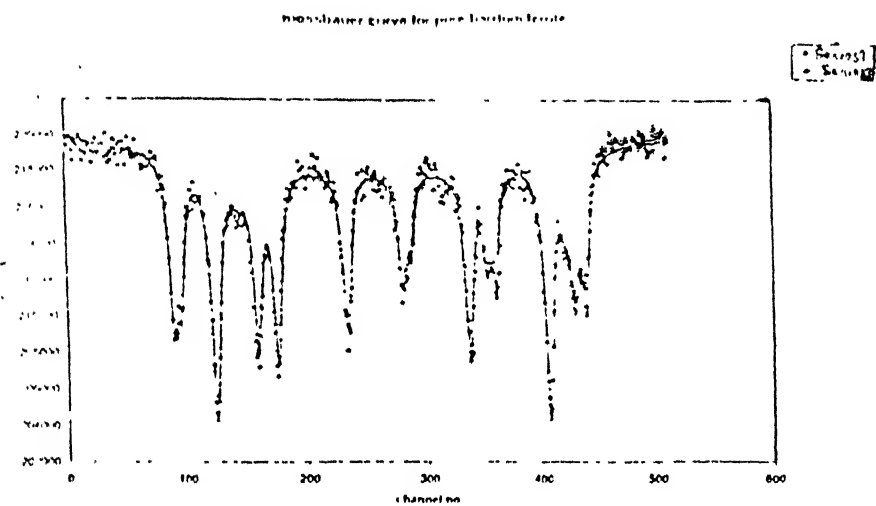
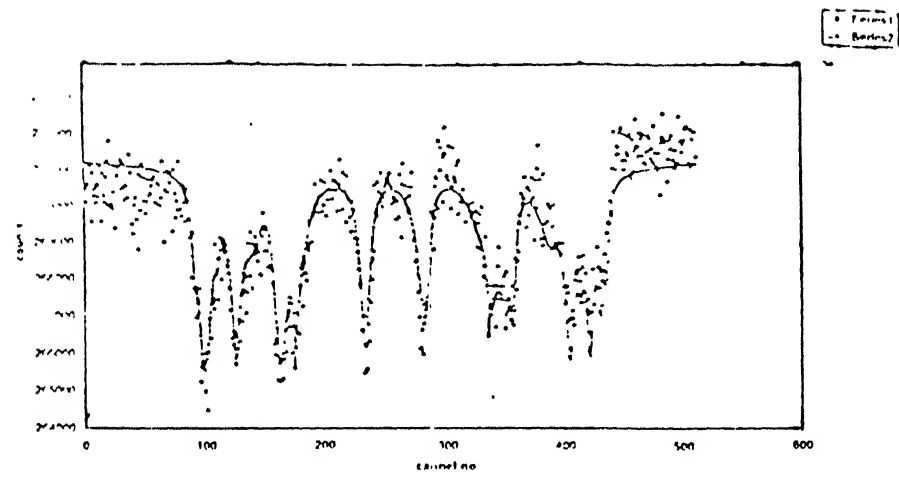
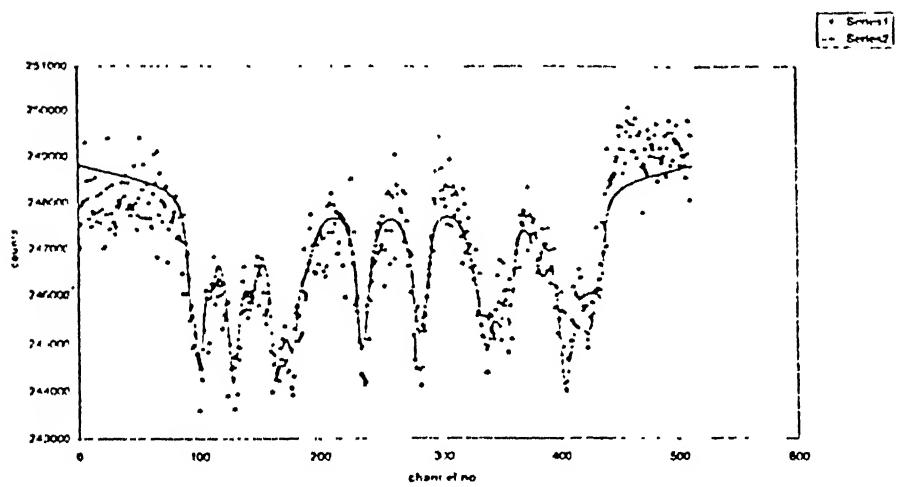


Figure 28. Mossbauer spectra of cobalt and titanium substituted barium ferrite $\text{BaFe}_{12-2x}\text{Co}_x\text{Ti}_x\text{O}_{19}$ ($x = 0, 0.2, 0.4$)



mossbauer curve for Co-Ti doping (0.8)



mossbauer curve for Co-Ti doping (1.0)

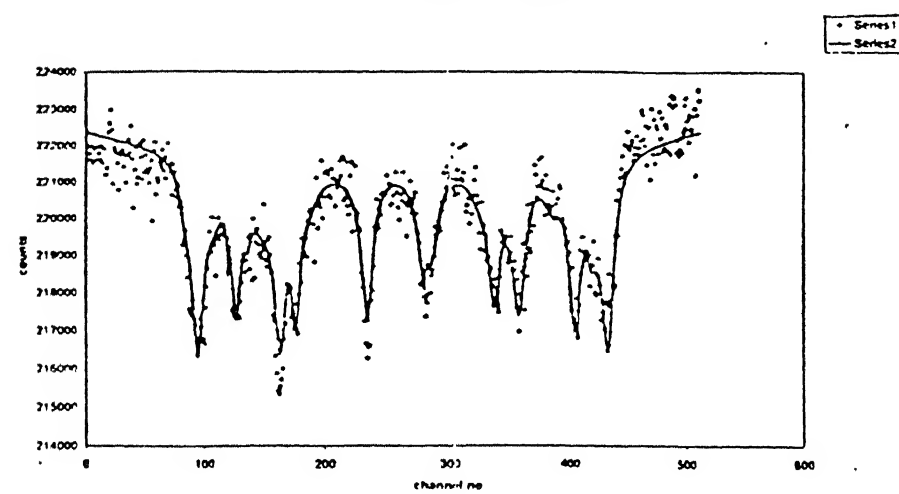


Figure 29. Mossbauer spectra of cobalt and titanium substituted barium ferrite $\text{BaFe}_{12-2x}\text{Co}_x\text{Ti}_x\text{O}_{19}$ ($x = 0.6, 0.8, 1.0$).

increase in Co-Ti substitution. Hyperfine fields remain nearly same for 12k and 2b sites. Exception to this description is rise in hyperfine fields for 2a and 2b sites for compositions corresponding to $x = 1.0$ and 0.4 , respectively. The area of sextets corresponds to the number of Fe^{3+} ions present at respective crystallographic site. The decrease in area of sextet of 12k, 2b and $4f_{iv}$ sites denotes the substitution of Co and Ti ions to these locations. Besides, there is no substitution of Co^{2+} and Ti^{4+} ions to $4f_{vi}$ and 2a sites. The significant decrease in hyperfine fields of $4f_{vi}$, 2a and $4f_{iv}$ sites indicate that the surrounding of Fe^{3+} ions there has changed and perhaps contain non-magnetic ion Ti^{4+} . This provides further evidence for substitution of Co^{2+} and Ti^{4+} ions at 12k and 2b sites. The isomer shift and quadrupole splitting for sextet corresponding to crystallographic site 2b are significant as compared to other sites in barium ferrite. Also, new fields appear in substituted compounds. There is a statistical probability that more than one non magnetic Ti^{4+} ions sit around some crystallographic sites which results in reduction of hyperfine fields of that sites significantly and which appear as a new field. Zhoes, Morrish and Li [31] have reported that new sub patterns k' and k'' results due to changes in the environment of iron ions at 12k site when substitution take place in R blocks. But it is difficult to ascertain sub patterns to the new hyperfine field in our case because of limited data available. Co^{2+} and Ti^{4+} ions are going preferentially to two up spin sites 12k and 2b and down spin site $4f_{iv}$ the overall effect is such that saturation magnetization varies marginally until substitution level is high. According to Albanese [24] the origin of uniaxial magneto anisotropy in $\text{BaFe}_{12}\text{O}_{19}$ lies in the iron ions of bipyramidal 2b and octahedral $4f_{vi}$ sites belonging to R block. In the present case, we find that 2b site is preferred by cobalt and cobalt-titanium ions in $\text{BaFe}_{12-x}\text{Co}_x\text{O}_{19-x/2}$ and $\text{BaFe}_{12-2x}\text{Co}_x\text{Ti}_x\text{O}_{19}$

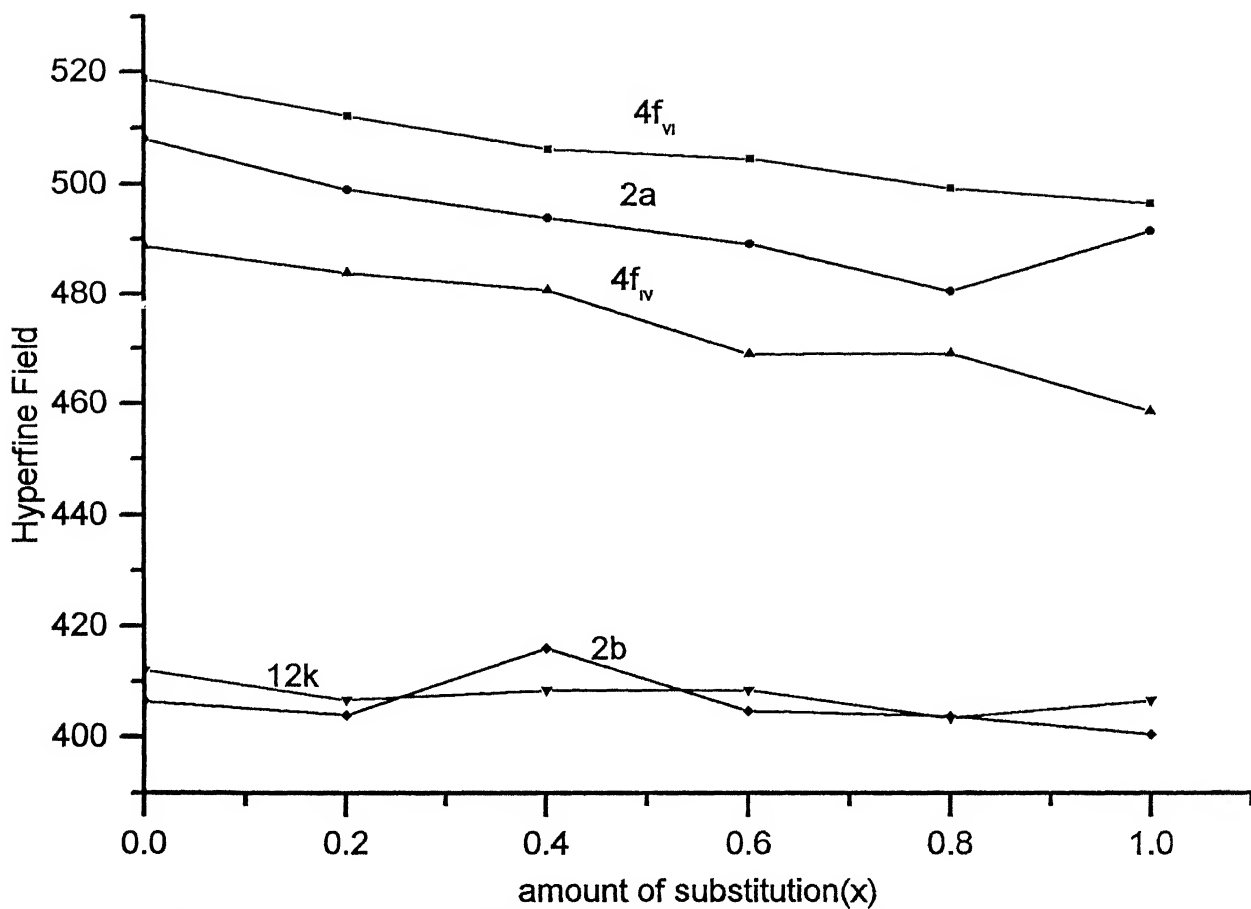


Figure 30 :Variation of hyperfine fields with Cobalt andTitanium content in $\text{BaFe}_{12-2x}\text{Co}_x\text{Ti}_x\text{O}_{19}$ ($x=0.2, 0.4, 0.6, 0.8, 1.0$)

respectively. Also, Ti^{4+} is a non-magnetic ion we therefore believe that substitution at 2b site is mainly responsible for reduction in magneto crystalline anisotropy and hence coercivity in cobalt and cobalt-titanium substituted barium ferrites. Kubo, Ido, Yokoyama and Koike [32] have prepared $\text{BaFe}_{12-2x}\text{Co}_x\text{Ti}_x\text{O}_{19}$ compounds by glass-crystallization method and shown saturation magnetization to decrease with decreasing particle size. This result was explained by assuming the existence of a few angstrom thick nonmagnetic layer on the surface of the particles, thereby causing increase in the non-magnetic volume fraction. Further, the coercivity dependence on particle size follows either super paramagnetism theory or multi domain nucleation mechanism.

Turilli, Licci, Rinaldi and Reriu [33] have synthesized $\text{BaFe}_{12-2x}\text{Mn}_x\text{Ti}_x\text{O}_{19}$ ($0 < x < 2$) by mixing stoichiometric oxides and carbonates using ceramic route and found saturation magnetization to remain unaffected upto $x=0.4$. The large perturbation of the magnetic order was however, observed in samples corresponding to $x>0.5$ and this was attributed to the preferential occupation of the crystallographic site 12k by both the Mn^{2+} and non-magnetic Ti^{4+} ions.

Hong, Paig, Agresti and Shelfer [34] introduced a low-temperature, ambient pressure coprecipitation method to prepare $\text{BaFe}_{12-2x}\text{M}_x\text{Ti}_x\text{O}_{19}$ ($0 < x < 2$; $\text{M} = \text{Ti}^{4+}$ or Mo^{4+}). The resulting particles were of hexagonal platelet shapes of size 0.1-0.6 μm diameter. While the saturation magnetization was found to be independent of local crystalline order, coercivity could be controlled in the range 500-1400 Oe. The monotonic

decrease of relative intensities of the 12k sites with concentration in Mossbauer spectra of Co-Mo substituted samples suggest preferential occupancy of this very location with little distortion in the crystal structure. Agresti and Shelfer[34] later obtained well-resolved Mossbauer spectra of $\text{BaFe}_{12-2x}\text{Mo}_x\text{Ti}_x\text{O}_{19}$ ($0 < x < 2$) samples and observed again substitution of 12k crystallographic sites of iron by Co-Mo ions.

According to Zheng and Jian-shang [35] barium ferrites of desired magnetic properties and particle size (suitable for perpendicular magnetic recording) could be produced by glass crystallization method by choosing the amount of substitution x and crystallization temperature in the $\text{BaFe}_{12-2x}\text{M}_x\text{Ti}_x\text{O}_{19}$ system. The increase of the Co-Ti content and decrease of crystallization temperature have led to decrease in the coercivity value. Such an observation interpreted as changes occurring in the crystallization energy of $\text{BaFe}_{12-2x}\text{Co}_x\text{Ti}_x\text{O}_{19}$ with the substitution x .

Zhou, Morrish, Li and Hong [31] showed that Co^{2+} and Ti^{4+} cations preferably occupy the $4f_{vi}$ and 2b crystallographic sites and significantly weaken the exchange interaction between iron ions and hence uniaxial anisotropy, leading thereby to decrease in coercivity and lowering of curie temperature with increasing x in $\text{BaFe}_{12-2x}\text{Co}_x\text{Ti}_x\text{O}_{19}$ ($0 < x < 0.9$) samples, synthesized by ceramic method. In contrast, the present investigation suggests preferential substitution of 12k and 2b crystallographic sites by Co^{2+} and Ti^{4+} ions.

It is worth noting that others have reported different site preferences for the Co^{2+} and Ti^{4+} ions. Examples are the octahedral 12k, $4f_{vi}$

and 2a, 12k sites and 2b sites [31]. Though the site preference usually depends on the nature of cation, yet, it may deviate with the preparation method. Further studies are required to resolve these differences.

CONCLUSION

1. Auto ignition method can produce cobalt and cobalt-titanium containing barium hexaferrites of compositions $\text{BaFe}_{12-x}\text{Co}_x\text{O}_{19-x/2}$ ($0 < x < 1.6$) and $\text{BaFe}_{12-2x}\text{Co}_x\text{Ti}_x\text{O}_{19}$ ($0 < x < 1.0$) for magnetic recording applications.

2. $\text{BaFe}_{12-x}\text{Co}_x\text{O}_{19-x/2}$ exhibits the magneto plumbite hexagonal structure upto substitution $x=1.6$. In addition, product contains another phase of composition $\text{Ba}_2\text{Co}_2\text{Fe}_{12}\text{O}_{22}$ when cobalt content (x) becomes 1.2 or more. Curie temperature of these phases are $460\text{--}441^\circ\text{C}$ (decreases with cobalt content upto $x=1.2$) and 323°C , respectively.

Coercivity (H_c) value decreases significantly with increase of cobalt content in $\text{BaFe}_{12-x}\text{Co}_x\text{O}_{19-x/2}$ compounds, viz., H_c values are found are 4223 Oe and 2072 Oe for $x=0$ and 1.6, respectively. However, saturation magnetization (M_s) initially increases marginally but decreases beyond the substitution level of $x=1.2$ possibly due to emergence of another phase.

Mossbauer spectra reveal substitution of iron by Co^{2+} ions preferentially at 12k, 2b and randomly at 4 f_{iv} , 2a and 4 f_{vi} crystallographic sites. However, hyperfine fields of all the sites except '2b' decreases with increase in substitution content.

3. The Curie temperature (T_c) and coercivity values (H_c) decrease sharply while saturation magnetization (M_s) either remain constant or decrease marginally with increase of Co-Ti content (x) in $\text{BaFe}_{12-2x}\text{Co}_x\text{Ti}_x\text{O}_{19}$ compounds ($0 < x < 1$). The T_c , H_c and M_s values for $x=0$ and 1 are 460 and 362°C , 4223 and 407 Oe, 58.8 and 56.2 emu/gm, respectively.

The significant decrease in T_c and H_c values can be attributed to preferential substitution of iron by Co^{2+} and non-magnetic Ti^{4+} ions at 12k, 2b, 4 f_{iv} crystallographic sites. Also, hyperfine fields of 12k and 2b sites remain independent while that of 4 f_{vi} , 2a and 4 f_{iv} sites decrease with increase in substitution level.

4. By adjusting the $\text{Co}^{2+}\text{-Ti}^{4+}$ ions content (i.e, the value of x) in $\text{BaFe}_{12-2x}\text{Co}_x\text{Ti}_x\text{O}_{19}$, it is possible to obtain material of desired characteristics for magnetic recording media applications. For example, products with $x=0.4\text{--}1.0$ exhibit coercivity and saturation magnetization in the range of $1600\text{--}407$ Oe and $61.1\text{--}56.2$ emu/g, respectively.

References:

- [1] J.C.Mallison, " *The foundations of magnetic recording*", Academic Press, San Diego, cA (1987)
- [2] G.Bate, " *Particulate recording materials*", Proc. IEEE, 74, 1513 (1986)
- [3] S.Iwasaki and K.Takemura, " *An analysis for circular mode of magnetization in short wavelength recording*", IEEE Trans. on Magnetics, vol 1,no-5, 1173 (1975)
- [4] T.Suzuki, " *Perpendicular magnetic recording - its basic and potential for future*", IEEE Trans. on Magnetics, mag -20, 675 (1984)
- [5] J.R.Dessere " *Crucial points in perpendicular recording*", IEEE Trans. on Magnetics, Mag -20, 545(1985)
- [6] S. Iwasaki and Y. Nakamura, " *An analysis for magnetization mode for high density recording*", IEEE Trans. on Magnetics, Mag-13, 1272 (1977)
- [7] T.C. Arnoldussen, " *Thin film recording media*", Proc. IEEE vol-74, 1526 (1986)
- [8] W.A.Kaczmark and B.W.Ninham, " *Magnetic properties of barium ferrite powders prepared by surfactant assist ball milling*", IEEE Transactions on Magnetics, 30, 717 -719 (1994).
- [9] N.K.Ghosh, " *Preparation characterization and magnetic property measurements of co-precipitated Barium ferrite powders*", M.Tech. thesis, Dept of Metallurgy, I.I.T., Kanpur (1980).
- [10] I.J.McColm and N.J.Clark, " *Forming, shaping and working of high performance ceramics*", 1-338, Blackie, Glasgow (1988).
- [11] P.Gornert, E.Sinn, W.S.Chuppel et al., " *Structural and magnetic properties of $BaFe_{12-2x}Co_xTi_xO_{19}$ powder prepared by glass crystallization method*", IEEE Trans. on Magnetics, Vol-26, no-1, 12-14, (1990)

- [12] D. Rambabu, " *An efficient combustion process for synthesis of $\text{YBa}_2\text{Cu}_3\text{O}_7$* ", Jpn. J. Appl. Phys, 29, 507-508 (1990).
- [13] P. Sujatha Devi and H.S. Maiti, " *A novel autoignition combustion process for the synthesis of Bi-Pb-Sr-Ca-Cu-O super conductors with a $T_c(0)$ of 125K*", Journal of Solid State Chemistry, 35-42 (1994).
- [14] J.F. Knowles, " *Magnetic properties of individual acicular particles*", IEEE Trans. on Magnetics, mag-17, 3008 (1981)
- [15] U. Kullman, E. Koster and B. Meyer, " *magnetic anisotropy of Ir doped CrO_2* ", IEEE Trans. on Magnetics, mag-20, 742 (1984)
- [16] A.E. Berkowitz, F.E. Parker, E.L. Hall and G. Podolsky, " *Toward a model for co-surface treated Fe oxides*", IEEE Trans. on Magnetics, 24, 2871 (1988)
- [17] S. Umeki, " *A new high coercivity magnetic particle for recording tape*", IEEE Trans. on Magnetics, mag-10, 655 (1974)
- [18] M. Kishimoto, " *On the coercivity of cobalt ferrite epitaxial iron oxides*", IEEE Trans. on Magnetics, mag-17 3029 (1989)
- [19] M.P. Sharrrock and L.W. Carlson, " *The application of barium ferrite particles in advanced recording media* ", IEEE Trans. on Magnetics, mag-31, 2871 (1995)
- [20] Hans Jur gen Pitcher and R.J. Veitch, " *Advances in magnetic tapes for high density information stage*", IEEE Trans. on Magnetics, mag-31, 2883 (1995)
- [21] R. Valinuela, " *Magnetic Ceramics*", Cambridge Univ. press (1994)
- [22] B.D. Cullity, " *Introduction to magnetic materials*", Addison Wesley publishing company (1972)
- [23] D.F. Eagle and J.C. Mallinson, " *On The Coercivity of $\gamma\text{Fe}_2\text{O}_3$ Particles*", Journal of Applied Physics vol.38 (3) 995-997, March 1967.
- [24] G. Albanese, " *Origin of uniaxial magneto-crystalline anisotropy of $\text{BaFe}_{12}\text{O}_{19}$* ", de physique, 38, CI-85 (1977).

- [25] M.Kishimoto and S.Kitahata, "*temperature dependence of anisotropy field in Co-Ti substituted Ba-ferrite particle*," IEEE Trans. Magn. , Vol. 25, 4063-4065, Sept. 1989.
- [26] P.G.Prasad, "*Studies of metal substituted barium ferrites synthesized by a novel auto ignition method for ultra hig density recording applications*" M.Tech. Thesis, Department of Material Science, IIT Kanpur, 1998.
- [27] James Read, "*Introduction to the principal of ceramic processing* ", John Wiley and Sons (1988).
- [28] $Ba_2Co_2Fe_{12}O_{22}$, 1996 JCPDS-International centre for diffraction data.
- [29] J.P.Chen, C.M.Sorensen, K.J.Kalbunde, G.C.Hadjipanayis, E.Devlin and A.Kostikas, "*Size-dependent magnetic properties of $MnFe_2O_4$ fine particles synthesized by coprecipitation*" Vol. 54, Number 13, Physical Review B, 9288-9296, 1 October 1996
- [30] E.P.WOHLFARTH "*Ferromagnetic Materials*" Vol.3, North-Holland Physics Publishing, 1000 AC Amsterdam, The Netherland.
- [31] X.Z.Zhou, A.H.Morish and Z.W.Li, "*Site preference for Co^{3+} and Ti^{4+} in Co-Ti substituted barium ferrite*", IEEE Trans.Mag. , Vol.27, No.6, 4654-4656 Nov.1991.
- [32] O.Kubo, T.Ido, H.Yokoyama, and Y.Koike, "*Particle size effect on magnetic properties of $BaFe_{12-2x}Ti_xCo_xO_{19}$* " J.Appl.Physics 57(1), 15 4280-4282, Apr.1985.
- [33] G.Turilli, F.Licci, S.Rinaldi and A.Deriu " *Mn^{2+} , Ti^{4+} substituted barium ferrite*" Journal of Magnetism and Magnetic Materials 59(1986) ,127-131, North-Holland, Amsterdam.
- [34] D.J.Agresti, T.D.Shelfer, Y.K.Hong and Y.J.Paig, "*A Mossbauer Study Of CoMo- Substituted Barium Ferrite*" IEEE Transactions On Magnetism, Vol.25, No.5, 4069- 4071, September 1989.
- [35] Yang Zheng and Liu Jian-zhong, "*Preparation And Magnetic Properties Of Co And Ti Substituted Ba-Ferrite Fine Platelet Particles*" IEEE Transactions On Magnetism, Vol. Mag-23, No.5, 3131-3133, September 1987.